Review #1

SUMMARY

This is my second review of this paper, which describes a GPS-based technique to make estimates of basal mass balance (BMB) and surface mass balance estimates for Pine Island Glacier ice shelf (PIGIS). The inclusion of GPS-derived snow surface height relative to the GPS antenna is a particularly interesting addition to standard ice-shelf GPS analyses, and the results are tied in well to other utilized datasets including the stereo-imagery of the DEM and the surface snow/firn state from a RACMO-based firn density model (FDM).

The paper is much clearer than the previous version, due largely to simplifying the set of vertical coordinate variables.

Specific comments are divided into “Major”, where I’d like to know what you did in response, and “Minor”, which don’t require documentation in revision. Numbers refer to original page.line.

-- Laurie Padman

GENERAL COMMENTS

1. I think “PIG shelf” should always be “PIG ice shelf”, in which case you might want to introduce “PIGIS” early and always use it.

We do not want to introduce additional acronyms and feel that "PIG shelf" is sufficient.

2. I don’t like the constructions “between/from 2012-2014” as it requires reading the dash as “and” or “to”. Better to replace the dash with a word, or say “the period 2012-2014”. Similarly for ranges of dimensional values.

We changed most of these instances to "the period 2012–2014" but chose to leave some for simplicity. We consistently use the em-dash for ranges, which implies "to" in this context.

3. I’d try to avoid the construction “Figure X shows that …”. It suggests that a pre-existing set of figures is driving the paper, rather than the figures supporting the facts. It’s usually possible to say something like “The elevation at each site (Figure X) …”

This is stylistic and does not change the meaning of the text. We left as is.

MAJOR COMMENTS

3.20-3.22: You almost, but didn’t quite, finish the mass balance statement for the ice shelf itself. If 95-101 GT/yr for basal melting is 70-80% of mass loss from the ice shelf, then calving is 20-30 Gt/yr (although Rignot et al. 2013 says 62 Gt/yr), and SMB is 5 (Rignot). Does that add up to give the observed thinning rate?

Part of the confusion on this point is related to numbers from different time periods and different techniques. The estimates from Rignot et al. 2013 have been refined by more recent studies as cited in the text. A more thorough discussion of these numbers is presented in [*Shean*, 2016], and will be published in forthcoming papers.

4.32-4.34: Both bedrock GPS sites are outside the domain for Figure 1, right? Are they good choices, and are there different penalties for the different sites? Regardless, maybe tell us the typical distance away from the ice shelf GPS for each site.

We included distances in an earlier version, but removed to simplify this portion of the text. We reinserted to accommodate the reviewer's request. The HOWN site is far from the PIG shelf, but it was the best available base station data for 2008-2010.

5.2-5.3: I don't understand why you subset the 30-s positions to 10-minute intervals: you're throwing away 95% of the data?

This was done to reduce data volume and does not impact our results. Given the horizontal velocities of ~10 m/day, the displacement of the receivers over 15-second intervals is negligible. Even 10-minute intervals could be considered overkill for some analyses over a 2-year period.

5.11-5.18: This question was asked by both reviewers last time around: Why use a tide model when your data contains the exact tide, and the records are long enough to analyze? I'd expand this to suggest that a better IBE correction might be possible following Padman et al. (2003) rather than just using 1 cm/hPa. The correlation of the height data with the pressure from ERA-Int or the AWS would give you a better model. If you continue to use CATS2008, then a better expression for citing it is "an updated version of the model described by Padman et al. [2002]"

We updated the CATS2008 citation text, and we do cite the Padman et al (2003) paper. As specified in our original response to reviewers, the suggestion to redo the entire analysis with a different tide model or tide removal approach would not change our results. We appreciate the reviewer's comments and will consider this for future work.

7.22 and elsewhere: I am not familiar with NMAD. (1) You need to tell us something about it (what does it tell you that RMS doesn't), and (2) does it have units? If so, why "normalized" ?

NMAD is a robust metric of variability, less affected by outliers than std or rms.
https://en.wikipedia.org/wiki/Median_absolute_deviation
For the normal distribution, the "normalized" MAD (i.e. MAD multiplied by constant scale factor of 1.4826) is consistent with the standard deviation.
This is a standard statistical metric and we do not feel it requires further discussion in the text.

8.4-8.8: (1) v_fc is fairly important in your study, but there's not much information here to understand it other than calling it "dry firn compaction". My possibly wrong interpretation is that it is the height change associated with firn compaction *below* the pole base, and that this rate is set by the amount of new SMB above the pole base. But this needs to be clearer, and I'd also

want to know how the choice of a fixed “firn air content” of 12 m relates to what v_fc can be. (2) related: How does all this get us to an estimate of uncertainty on v_fc?

We include references to [*Ligtenberg et al.*, 2011] which contains a much more thorough description of v_fc and its uncertainty. This is beyond the scope of the current paper.

v_fc can be estimated for any layer in the firn column. In this paper, we estimated v_fc for a layer at the depth of the pole base over time. The reviewer is incorrect – loading from new SMB above the pole base has limited influence on v_fc. Rather, v_fc is primarily controlled by compaction rates in the underlying firn column, which are related to cumulative SMB history.

Regardless, based on feedback from both reviewers, and further discussion with coauthors, we decided to remove the discussion of v_fc from the text.

9.3-9.8: This is confusing as, at first thought, the relationship of the pole base to the moving firn-ice transition is not obvious. I think I understand v_fc now (see previous comment), but then the assumption of constant firn air (12 m) creates a relationship between the firn-ice transition and the total mass content of the firn layer, implying that compaction for the firn layer depth range under the pole base is determined by recent precip above the pole base.

We again refer the reviewer to [*Ligtenberg et al.*, 2011], which contains a more detailed discussion of IMAU-FDM. The firn model simulations do not involve a moving firn-ice transition, and do not require constant firn air. The latter was introduced as a simplification for the basal melt rate derivations in Section 3, which we justify in the text "limited temporal variability (+/-0.3 m or ~1-3%) in modeled IMAU-FDM total firn air content for the three PIG shelf grid cells during the relevant ~2-year study periods."

In the model, additional surface accumulation/ablation will result in total firn column thickness change, which will involves surface elevation change above the firn-ice transition.

9.13-9.14: The density ratio term in eq. (7) explains why you say that BMB is 9 times more sensitive to z_surf than to adot. However, this ignores the scaling of div.u and the relationship between z_surf and adot. Set divergence to zero, on a flat ice shelf with no BMB, and z_surf relates to adot, but the divergence term doesn’t even show up.

We are not ignoring div.u scaling, we are merely stating that "basal melt rates are ~9 times more sensitive to surface elevation change (Dz_{surf}/Dt) than SMB ($\dot{a}$) for a floating ice shelf". The divergence term is very small (as supported by observations presented in the text), but scaling of that term is also 9x larger than adot. As for the reviewer's comment about a flat ice shelf - if bdot is 0 and div.u is 0, then we are left with (Dz_surf/Dt)(~9) = adot.

10.28-10.29: Not “in the upper few meters of the firn column”, just “in the firn column above the pole base”. Right? What happens *below* the pole base doesn’t affect the antenna to surface distance.

This is correct. The "upper few meters" and "above the pole base" are synonymous in this case. We reworded to clarify:

"All GPS array records show an abrupt antenna-surface distance increase (~0.2–0.3 m) between December 2012 and January 2013, which is consistent with surface melting and/or enhanced firn compaction rates above the pole base (i.e., upper few meters of the firn column). "

12.10-12.12: This seems a bit disingenuous. The signal is being interpreted entirely as though all the assumptions are correct. You explain later (Section 5) that there are reasons it might be wrong, especially Section 5.1, but the uncertainties need to be addressed briefly here.

The magnitude of the melt rate differences between these sets of receivers is significantly greater than the measurement uncertainty. We feel that the organization presenting basic observations in this section, and discussing the details of uncertainty in later sections is appropriate.

13.10-13.17: This is not very convincing (to me). My reading of your paper, without being steeped in the PIGIS literature, is that longitudinal extension might be biased towards transverse basal channels, and that hydrostatic equilibrium of short scales might be being slowly approached over the decade since the ice began to float. Can you really resolve the dynamic term, given the scales of the transverse rifts seen in the right-hand panels of Figure 10?

This section was added to the first revision to address the other reviewer's concerns about hydrostatic equilibrium for channels/keels with length scales of ~1-2 km. It is not intended to address the length scales of the transverse rifts brought up by the reviewer. These issues are addressed in Section 5.4 on "Strain rate length scales"

15.10-15.11: Maybe I don't understand this all well enough; but in what way is PIG2 SMB "in balance with" ongoing firn compaction and basal melt during this period? In mass, or height? It seems like the balance is that ~2 m per year of fresh firn is deposited, but Table 1 suggests BMB is ~2 or ~4.4 m/yr (depending on method) of ice, and BMB is only ~1 m.w.e. per year, so it's only a balance in terms of thickness. But then compaction is fixed to only allow 12 m of firn air at all times?

The full sentence was "The limited variability in surface elevation at PIG2 (Figure 7C) suggests that the observed 2008–2010 SMB over the South PIG shelf was approximately in balance with ongoing firn compaction and basal melt during this period."

So, "surface elevation" involves height. Essentially, we are saying Dz_surf/Dt is close to zero for these years, so other terms in Equation 5 must be equal. As stated earlier, compaction is not fixed and we removed the language "ongoing firn compaction," which should hopefully address the reviewers concern.

The modified text reads "The limited variability in surface elevation at PIG2 (Figure 7C) suggests that the observed 2008–2010 SMB over the South PIG shelf was approximately equal to basal melt during this period, assuming negligible velocity divergence for this location. "

15.16: You can't say "appear to be uncorrelated". You either mean just "unrelated" (or "causally unrelated"), or you calculate the correlation and decide if it passes a statistical threshold or not.

We said "appear uncorrelated" but did not make the direct claim that they were "statistically uncorrelated". Changed to "unrelated"

16.11-16.31: I recommend rolling these two subsections together, and starting with the discussion of spatial variability so that, when you compare with the two direct measures of BMB, you already have the justification explained.

We are satisfied with the current organization and feel these two sections should be separate.

16.33-17.3: "that appear to display a lagged …". If this is true, then show it. However, once you start the sentence "Our analysis …", you seem to be stepping away from accepting the lagged correlation with ocean T. Overall, you seem to set up a belief that the ocean matters and that you have evidence for it, but then say "Actually, no, it's something else."

We modified to clarify that the first sentence is the assertion of [*Christianson et al.*, 2016]:

"Christianson et al. [2016] suggest that the subtle (~2–4%) changes in 2012–2014 GPS velocity display a lagged correlation with observed variations in ocean temperature records from moorings in Pine Island Bay (see Figure 1 for location), potentially implying causality."

MINOR COMMENTS

1.27: "limited" is unnecessarily vague here.

We feel this is appropriate for the abstract, and present details in the text.

2.6: "relatively coarse grid". By most standards, these grids are fairly "fine". You need to tell us what grid you need, and why.

We do specify desired SMB resolution (<1-km) and why in Section 6.7. We do not feel this belongs in the introduction.

2.7-2.8: This sentence seems to imply that installing GPS (the topic of this paper) is easier than these are things, but the logistics are similar.

We are not implying that GPS is easier, merely stating that field installations are logistically challenging. The ability to extract new information from existing GPS installations expands available options for cal/val without additional fieldwork.

2.10: Why "cumulative" balance?

A small bias in seasonal or annual mass balance observations can lead to large cumulative errors over time.

2.22-2.23: dynamic firn models are forced by a lot more than just SMB.

The text does not imply that modeled SMB is the only forcing.

2.35: “temporally dense” seems complicated: Why not just say “continuous” ? Overall, the issue is whether the single-to-noise combined with sampling characteristics gives you more valuable results than other methods at time *and space* scales you want to resolve.

We changed "temporally dense" to "continuous" and keep the later sentence that states "This approach yields temporally dense records of basal melt rates at spatially sparse GPS locations…", which is the point we are trying to make.

3.16: This net mass loss (40-50 GT/yr) applies to the entire PIG grounded-ice catchment, right?

Yes, we modified to read "net mass loss estimates of 40 to 50 Gt/yr for the full PIG catchment".

4.2: Don’t see the need to hyphenate “ice sheet” and “ice shelf” here

We hyphenated because both are used prior to "dynamics" (i.e., "ice-sheet dynamics" and "ice-shelf dynamics"). Defer to TC editorial staff.

4.27: As expanded upon, “fortuitous” seems like the opposite of what you mean!

Deleted "fortuitous"

4.29: I don’t understand the ‘(co)’

Deleted "(co)"

5.8-5.9: What are the “8 km GPS paths”? Do you mean “receiver separations”?

No. We modified to clarify:

"Absolute geoid errors are poorly constrained for coastal Antarctica, but relative geoid error for the cumulative horizontal displacement of the GPS array (~8 km over the 2-year period) should be <1-2 cm"

6.30 (but check everywhere): Consistent use of italics for Lagrangian derivative D/Dt. Note that some oceanography texts would say D{\itX}/D{\itt}.

They are consistent. We defer to TC editorial staff for preferred formatting.

8.21: If rho_ice =917 +/- 5, then how can you use 917 as the threshold for identifying the height of the firn-ice transition? Doesn’t that become a noisy estimate?

The +/-5 kg/m3 was not used with FDM, but is used for uncertainty calculations elsewhere in this paper (i.e., related to hydrostatic scaling term). We refer the reviewer to [*Ligtenberg et al.*, 2011] for details on the FDM use of 917 for this transition.

8.23: units for ‘d \approx 12 *m*’

Good catch. Changed.

9.24: The sign of the shear “dextral (right-handed)” doesn’t tell me anything. All I care about is that velocity is higher towards the center of the trunk flow, right?

Yes, we present magnitude and specify direction as dextral.

10.9-10.10: I really don’t like the format “increased (decreased) … increase (decrease)”. First, it’s hard to read. Second, it’s obvious, right?

We are confident that most readers are familiar with this presentation, and defer to TC editorial staff.

No, this is not necessarily obvious. If the entire array speeds up uniformly, there may not be any change in intra-network strain rates.

11.11: Italics for z_surf etc.

Again, good catch. Changed.

11.19-11.20: I don’t think you mean “scaled” temperatures; you mean “calibrated” temperatures, or local temperatures estimated from the relationship between PIGIS AWS and Evans Knoll.

Changed to "calibrated".

11.27-11.29: Would have preferred to see a graphic of the historical context for warm periods in a longer time range. Seems important, especially if it figures into total firn state.

This is beyond the scope of this manuscript, but we include the 1979–2016 ERA-Interim 2-m T record here for completeness. Top panel shows full temperature scale, bottom panel shows zoomed y-limits of approx. +/- 2°C.

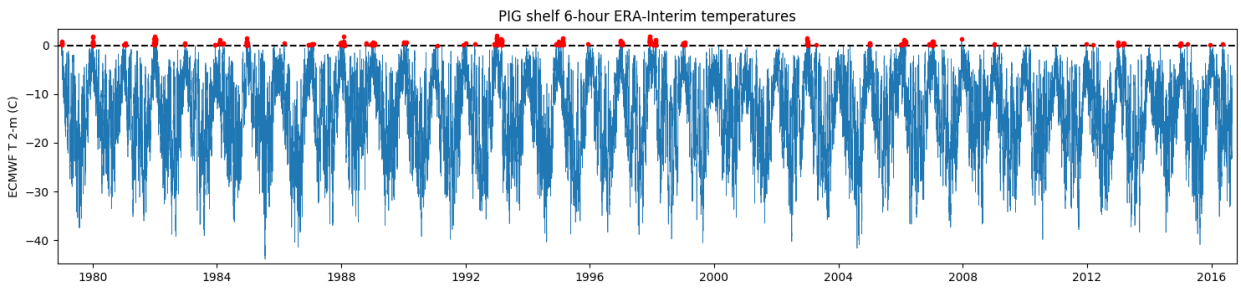

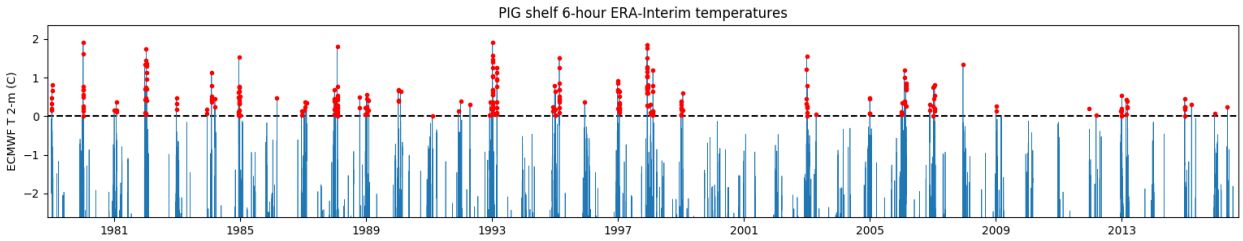

14.2: “We now consider the possibility that” => “It is possible that” ?

Changed to "We now consider whether…"

14.13: “Finally, we assume that …” Out of style with this section, which starts each para with a discussion fo what could go wrong, not what you assumed. So here, maybe “It is possible that the poles tilt over time.”

We modified the introductory sentence to include all three potential issues:

"We now consider whether some of the observed Dz_{surf}/Dt could be related to settling, heating, or tilting of the GPS poles over time."

14.33: My reading is that v_fc represents “firn compaction below the pole base”, not total firn compaction.

v_fc is the downward velocity due to firn compaction for a layer in the firn column, in this case, the layer containing the pole base.

16.4-16.5: *Why* is there missing antenna-surface distance data during this period? What causes loss of this valuable information?

This was addressed in Section 2.3 "The SOW3 record was curtailed on August 22, 2013, when antenna-surface distance decreased below the minimum threshold of ~0.5 m (Nievinski, 2013)."

We added "(see Section **Error! Reference source not found.**)" here for clarification.

17.27: spell out “cal/val”

Changed to "calibration/validation"

17.30: “Set GPS elevation mask to 0^o”. Only makes sense if you tell/remind us what the present setting is, and *why* that’s the present setting; i.e., is there a penalty on other measurements when you change the mask specifically for antenna-to-surface heights?

Changed to "set the GPS elevation mask to 0° (default values are typically ~5–10°)"

Setting to 0° potentially introduces more multipath noise from low elevation satellites for position estimates, but this filter can also be applied during post-processing.

18.3: Does NMAD have units?

The text reads "NMAD of ~0.57 m". No change is necessary.

FIGURES

See RC1 for some other figure comments.

F.4: This figure would be a good place to define v_fc.

The first round of reviews suggested that this figure was too complicated, with too many variables.

We simplified the text and removed much of the discussion around v_fc, so no change is necessary.

F.6: What does “annualized velocity magnitude” mean, when it clearly isn’t “annualized”?

This was an attempt to state that we scaled the 42-day displacement to m/yr. Removed "annualized" to avoid confusion.

F.7 and F.9: full-page-width would be good. Especially for Fig. 9, where the text asks us to see short-time-scale events in the 2012-2014 period.

Agreed. Will bring up with TC typesetting staff.

Review #2

The authors have gone to some effort to redraft the manuscript along the lines suggested by the reviewers. The result undoubtedly represents an improvement over the earlier version. The overall structure now seems easier to follow and the reduction in the number of variables has helped considerably. I also found the sections discussing the issue of isostatic equilibrium and stability of the poles useful. They remove many of the doubts from my mind about the results. However, in places I still found it hard to follow what the authors are actually trying to present.

1) The section I struggled with most was number 3, which apparently derives two expressions for the basal mass balance. The reason for using two expressions in never entirely clear, while the derivations are a little unsatisfactory.

In Section 3, we stated "The effects of processes that drive short-term surface-elevation change (e.g., accumulation, melting) are largely absent below the upper few meters of the firn column." In other words, z_surf includes variability due to SMB. This is not the case for z_ant, which is useful for isolating subtle variability in the basal melt signal. This is clear in Figure 9 A and B, and the caption included the sentence "Note limited residual magnitude and dampened seasonal signal of z_{ant} compared to z_{surf}. Unlike z_{surf}, no significant change is observed in z_{ant} from Dec. 2012 to Jan. 2013."

We felt this was clear, but we modified section 3 to address the reviewer's concern, and now present only one derivation for basal melt rates from surface elevation change. This change also addresses many of the reviewers concerns below.

For equations (1) to (5), the authors make a conventional assumption that the thickness of air within the firn is constant and can simply be subtracted from the total thickness to leave a solid-ice-equivalent thickness. That is fine, but raises a couple of questions:

(i) In what sense is (4) an approximation? Is it the assumptions of constant density that are subsequently made, but if so, why is (5) exact?

Assumptions about densities, firn air content, and hydrostatic equilibrium all contribute to uncertainty in the ice thickness estimates. We changed the ≈ to =, as the wording in revised manuscript is more explicit about assumptions for equation 5.

(ii) If it is OK to assume constant air content, which it appears to be, why worry about firn compaction at all? You could make the paper a whole lot simpler if you just left it at that. Is it considered because of the insight that the GPS records give into the process? If so, then it should really be given the same status as surface and basal mass balance in the title and abstract. It is an independent process that you are studying. The new section 3 now clarifies that you don't actually need it at all to derive basal mass balance.

As stated above, the GPS antenna elevation time series can potentially provide basal melt rate estimates without SMB variability in z_surf time series. To use z_ant, we need to account for

downward motion due to firn compaction (and other processes) in order to isolate the downward motion due to basal mass balance.

While we do feel that new information on firn compaction can be gleaned from the GPS records, we accepted the reviewers suggestion, and cut this from the paper. We hope to address this topic further in future work.

I struggled with equation (6). From Figure 4 it is clear that:

Z_ant = Z_surf + h_(ant-surf)

so the exact equation, from which the approximation in (6) is derived, has the total derivative of h_(ant-surf) on the right-hand side. That term is a combination of surface accumulation and compaction of the firn above the level of the (fixed) pole base.

This is a good point. The initial version of eq 6 was incorrect. We removed eq 6 from the paper.

This raises further questions:

(iii) What are the assumptions that you make to get to your version of (6)?

We removed eq 6 from the paper.

(iv) If these involve the assumption of steady accumulation and firn compaction, how is that distinct from the assumption of constant air content?

We removed eq 6 from the paper.

(v) Are equations (5) and (7) supposed to be independent? How can they be considered as such, when (7) still includes the surface elevation minus the air content?

z_surf is derived from two independent signals (z_ant and h_ant-surf). We compute linear fits to both observed Dz_ant/Dt and observed Dz_surf/Dt.

The previous eq 7 has been removed.

Overall, it would seem simpler to leave (5) as the source of the basal melt rates and discuss (6) in its exact and approximate forms in terms of the processes of firn compaction and how the model compares with the observation of the compaction velocity.

We maintain that there is value in considering basal melt rates derived from both Dz_surf/Dt and Dz_ant/Dt observations, but we implemented the reviewer's suggestion to limit basal melt rate derivation to eq 5, and leave most of the firn compaction and model evaluation discussion for a future paper.

2) The discussion of the derived melt rates is somewhat misleading. The authors mention the

50% reduction in melting reported by Dutrieux et al (Science, 2014), but those observations pre-date the GPS data discussed in this manuscript. I overlooked that in my earlier review, because I did not check back to the other papers. I should have done, but the text of this manuscript gave me no reason to suspect that the observations were not contemporaneous. I think that critical point should be clarified, and the relevance of those earlier observations should also be spelt out.

This is a good point - an oversight in an ongoing effort to split a long PhD thesis with a broader set of conclusions into discrete journal articles. The comparison with [*Dutrieux et al.*, 2014] belongs in a companion paper presenting a time series of annual DEMs used to derive 2008-2015 melt rates for the entire PIG ice shelf.

The exact date range for the 2012 observations in [*Dutrieux et al.*, 2014] is not specified in the manuscript or supplement (or we did not see dates upon review – presumably several different periods in Jan 2012?) The GPS records begin Jan 11, 2012, so presumably there is some overlap with the 2012 cruise observations. But not necessarily enough overlap to warrant a direct comparison.

We modified the text in Section 6.6 to address this oversight.

Are the authors assuming, based on Figure 2a of Christianson et al (GRL, 2016), that the variability through the observational period was as large as that before it? Maybe their results are telling them that the upper water column variability matters less for the melt rates?

We are only considering the variability during the periods when we have GPS observations.

In Webber et al (Nature Communications, 2017), the full ocean records are presented. In Figure 4 of that paper the eye is drawn to the upper water column variability that presumably dominates the average numbers in the Christianson et al figure. But deeper down you see a steady decline to January 2013, followed by a slight recovery. If temperatures at around 700 m are the critical factor, then most of the decline occurred in the period up to January 2012 (sampled by Dutrieux et al) and the variability through the period of the GPS records (discussed here) was much more muted. Could this explain the relatively steady melt rates observed? And how steady are they? Some of the lines seem to show a gradient that is reducing in the first part of the record, then increasing in the second part. Could that be consistent with slight cooling to 2013, followed by slight warming?

This is all valuable information and insight, but is beyond the scope of this manuscript. The GPS records tell us that basal melt rates at these sites did not vary during this period. Most of the interesting "why" questions would only involve further speculation on our part. We will take these useful comments into consideration as we finalize subsequent manuscripts on the subject.

The record that seems at odds with this interpretation is the altimeter record presented in Figure 2a of Christianson et al. Is that the same record as the one discussed here? Why is the temporal variability shown by Christianson et al now ignored?

Section 6.4 includes a discussion of the bottom altimeter data, and its limitations, which preclude a direct comparison (at least in the opinion of the first author).

3) Some more minor points:

(i) Page 1, Line 16: “To better understand …” Does the Cryosphere accept the split infinitive?

We defer to TC editorial team.

(ii) Page 3, Line 19: I don’t think I would describe the ice shelf as “large”!

Changed to "…terminates in an ice shelf ("main shelf")…"

(iii) Page 5, Line 28: Here you mention firn compaction above the pole base, but I don’t think you ever quantify this term do you? When you use the term v_cf, is it always compaction below the pole base, or is it sometimes the compaction over the whole firn column? It would help if you were clearer on this point.

v_fc can be estimated for any layer. Throughout the paper, we used v_fc as the downward velocity of a tracer at the pole base. Regardless, we removed most discussion of v_fc to reduce confusion.

(iv) Page 7, Line 5: Shouldn’t it be the “Regional Antarctic Climate Model”.

No, the text is correct.

(v) Section 6.1, paragraph 1: Here you need to be really careful about what you mean by firn compaction. You discuss the movement of Z_surf relative to its initial level. That is a function of surface accumulation and compaction above the initial level, isn’t it? But you seem to use a compaction velocity determined for the firn below the pole base? I’m afraid I don’t follow this.

As outlined in the response to reviewer comments submitted with revision v1 (See Figure 2), we also considered downward velocity of the z_surf0' tracer over time. This is different than the v_fc for the pole base tracer. This accounts for the effects of surface accumulation and near-surface compaction rates between z_surf0' and pole base layers.

(vi) Page 17, Line 19: Another split infinitive (“to further constrain”).

We defer to TC editorial team.

(vii) Page 18, Lines 4-9: Again, why should Z_surf-Z_surf0 be affected by firn compaction below the pole base? Both elevations change at the same rate as a result of deep compaction. Surely, only compaction between the two levels can affect the elevation difference?

This is a good point. We removed the reference to v_fc, so the text now reads:

"Surface elevation relative to a firn layer tracer for the initial surface (z_{surf} - z_{surf0}) increased at rates of ~0.8–1.1 m/yr for all GPS sites, which is consistent with modeled SMB of ~0.7–0.9 m w.e./yr and modeled downward firn-compaction velocities"

(xi) Page 18, Line 21: See comments under 2), above. How can you be so sure that the temperature variability was significant?

Changed to "substantial" although the observed changes are "significant" given the measurement uncertainty of the mooring T sensors.

GPS-derived estimates of surface mass balance and ocean-induced basal melt for Pine Island Glacier ice shelf, Antarctica

David E. Shean[1,2], Knut Christianson[3], Kristine M. Larson[4], Stefan R.M. Ligtenberg[5], Ian R. Joughin[1], Ben E. Smith[1], C. Max Stevens[3], M. Bushuk[6], D.M. Holland[7,8]

[1]Applied Physics Laboratory Polar Science Center, University of Washington, Seattle, WA, USA
[2]Department of Civil and Environmental Engineering, University of Washington, Seattle, WA, USA
[3]Department of Earth and Space Sciences, University of Washington, Seattle, WA, USA
[4]Department of Aerospace Engineering Sciences, University of Colorado, Boulder, CO, USA
[5]Institute for Marine and Atmospheric research Utrecht, Utrecht University, Netherlands
[6]Geophysical Fluid Dynamics Laboratory, Princeton University, Princeton, NJ, USA
[7]Courant Institute of Mathematical Sciences, New York University, New York, NY, USA
[8]Center for Global Sea-Level Change, New York University, Abu Dhabi, UAE

Correspondence to: David Shean (dshean@uw.edu)

Abstract

In the last two decades, Pine Island Glacier (PIG) experienced marked speedup, thinning, and grounding-line retreat, likely due to marine ice-sheet instability and ice-shelf basal melt. To better understand these processes, we combined 2008–2010 and 2012–2014 GPS records with dynamic firn model output to constrain local surface and basal mass balance for PIG. We used GPS interferometric reflectometry to precisely measure absolute surface elevation (z_{surf}) and Lagrangian surface elevation change (Dz_{surf}/Dt). Observed surface elevation relative to a firn layer tracer for the initial surface ($z_{surf} - z_{surf0}$) is consistent with model estimates of surface mass balance (SMB, primarily snow accumulation) and downward velocity due to firn compaction. A relatively abrupt ~0.2–0.3 m surface elevation decrease, likely due to surface melt and increased compaction rates, is observed during a period of warm atmospheric temperatures from December 2012 to January 2013. Observed Dz_{surf}/Dt trends (-1 to -4 m/yr) for the PIG shelf sites are all highly linear. Corresponding basal melt rate estimates range from ~10 to 40 m/yr, in good agreement with those derived from ice-bottom acoustic ranging, phase-sensitive ice-penetrating radar, and high-resolution stereo DEM records. The GPS and DEM records document higher melt rates within and near features associated with longitudinal extension (i.e., transverse surface depressions, rifts). Basal melt rates for the 2012–2014 period show limited temporal variability, despite large changes in ocean temperature recorded by moorings in Pine Island Bay. Our results demonstrate the value of long-term GPS records and interferometric reflectometry for ice-shelf mass balance studies, with implications for the sensitivity of ice-ocean interaction at PIG.

1 Introduction

The widespread availability of precise Global Positioning System (GPS) measurements has revolutionized the study of ice dynamics and glacier mass balance (e.g., Gao and Liu, 2001). Continuously operating dual-frequency GPS receivers provide high-frequency (1 Hz or less), highly accurate (<1-3 cm) measurements of position, which can be used to derive surface velocity and elevation change. For applications involving ice dynamics, these measurements offer important constraints for the mass continuity equation, which equates surface elevation change with ice flux

Deleted: Christianson[2]
Deleted: Larson[3]
Deleted: Ligtenberg[4]
Deleted: Stevens[2]
Deleted: Bushuk[5]
Deleted: Holland[6,7]
Deleted: Earth
Deleted: Space Sciences
Deleted: [4]Institute
Deleted: [5]Geophysical
Deleted: [6]Courant
Deleted: [7]Center

divergence, surface mass balance, and basal mass balance. Here, we explore a methodology to constrain each of these components directly from GPS observables.

Surface mass balance (SMB) processes include precipitation, sublimation, wind redistribution of surface snow, and melt water runoff. Regional climate models forced by reanalysis output now provide daily estimates of Antarctic SMB on a relatively coarse grid (~5.5 to 27 km). *In-situ* SMB measurements are, however, still essential for model calibration and validation. Traditionally, SMB is measured using stake networks, automated weather stations, near-surface radar surveys, and firn/ice cores, all of which require substantial field operations in remote locations. These measurements also tend to bias model calibration towards accessible locations, and recent studies indicate that these biases can significantly affect mass balance results, often resulting in overestimates of cumulative balance due to poor sampling in dynamic areas (Andreassen et al., 2016).

Antarctic firn/ice core records indicate that SMB variability over most of Antarctica during the last 800 years was statistically insignificant, but that accumulation increased more than 10% for high-accumulation coastal regions (e.g., the Amundsen Sea Embayment) since the 1960s (Frezzotti et al., 2013). Historically, these areas have been poorly sampled with traditional methods, providing limited data available for validation of modeled SMB.

Accurate knowledge of firn compaction and its spatiotemporal variability is essential for interpreting observed surface elevation change in remote sensing data (e.g., satellite altimetry), and for partitioning this change into components related to ice dynamics and SMB (e.g., Shepherd et al., 2012; Wouters et al., 2015). Depth-dependent compaction rates can be estimated from a number of different methods, including vertical strain measurements (Arthern et al., 2010; Hamilton and Whillans, 1998), borehole optical stratigraphy (Hawley and Waddington, 2011), repeat phase-sensitive radio-echo sounding (pRES) measurements (e.g., Jenkins et al., 2006) and ice-penetrating radar observations of internal layers over time (e.g., Medley et al., 2014, 2015). In the absence of these measurements, dynamic firn models forced by modeled SMB can provide estimates of compaction rates throughout the firn column, which can be integrated to obtain estimates for the contribution of firn compaction to surface elevation change over time (e.g., Ligtenberg et al., 2011).

Basal mass balance (BMB) for ice shelves (i.e., bottom melting, accretion) is driven by complex ice-ocean interaction. State-of-the-art ice-shelf cavity ocean circulation models offer some insight into sub-shelf ice-ocean interaction, but these models lack validation, as *in-situ* hydrographic observations are limited, especially within the sub-shelf cavity and the ice-ocean boundary layer. Some direct measurements are available from autonomous submersibles (e.g., Dutrieux et al., 2014) and instrumentation deployed through ice-shelf boreholes (e.g., Stanton et al., 2013), but available data are limited to short time periods and small spatial extents. Precise measurements of surface elevation change from remote sensing observations (e.g., laser altimetry, digital elevation models (DEMs)) can also be used to infer BMB (e.g., Dutrieux et al., 2013; Moholdt et al., 2014; Pritchard et al., 2012; Shean, 2016), but temporal resolution is limited, as time intervals between repeat observations are typically several months to years.

Here, we use continuous GPS records from the Pine Island Glacier Ice Shelf to constrain local SMB, flux divergence and BMB. We use changes in observed GPS antenna elevation and reflectometry-derived surface elevation to validate SMB/firn model output. Flux divergence is estimated from observed strain rates between GPS stations. These estimates are then used to isolate elevation change due to local BMB. This approach yields temporally dense records

Deleted: temporally dense

of basal melt rates at spatially sparse GPS locations, which are combined with high-resolution DEMs from the same time period to provide spatial context. These complementary results for the PIG ice shelf provide new information about the time-variable magnitude and spatial distribution of basal melting, offering indirect observations of ice-ocean interaction and BMB sensitivity to ocean heat content variability, with implications for other rapidly evolving "warm-cavity" Antarctic ice shelves.

1.1 PIG background

Pine Island Glacier is one of the largest and most dynamic ice streams in West Antarctica. Since the 1970s, PIG has experienced ~30 km of grounding line retreat along its centerline (Rignot et al., 2014) (~8 km average retreat across full width of fast-flowing trunk (Joughin et al., 2016)), a ~75% increase in surface velocity (Mouginot et al., 2014), and >100 m of thinning (Bindschadler, 2002; Pritchard et al., 2009), with accelerated retreat beginning in the 1990s. These changes have been attributed to some combination of geometric instability (i.e., marine ice sheet instability) and external forcing (i.e., increased ocean heat content and/or changes in sub-shelf circulation) (Jacobs et al., 2011; Joughin et al., 2010).

Present-day surface velocities are ~4 km/yr, with annual discharge of ~130–135 Gt (Medley et al., 2014; Mouginot et al., 2014) and net mass loss estimates of 40 to 50 Gt/yr for the full PIG catchment (Medley et al., 2014; Rignot, 2008). This mass loss is responsible for ~0.11 mm/yr global sea level rise (SLR), or approximately 40–45% of the total ~0.26 mm/yr Antarctic SLR contribution (Church et al., 2013; Rietbroek et al., 2016; Shepherd et al., 2012).

Figure 1 shows the fast-flowing portion of the PIG ice stream, which terminates in an ice shelf ("main shelf") that is ~25 km wide, ~100 km long, and ~1–1.5 km thick across the grounding line. Basal melting accounts for ~60–75% of mass loss from the ice shelf, with estimated 2003-2008 melt rates of ~95–101 Gt/yr (Depoorter et al., 2013; Rignot et al., 2013) and 2008-2015 melt rates of ~80-90 Gt/yr (Shean, 2016).

Deleted: a large

Deleted: 70–80

The main shelf has complex surface topography, including km-scale surface ridges and troughs that correspond to basal keels and channels, respectively (Bindschadler et al., 2011; Vaughan et al., 2012). A series of longitudinal (along-flow) ridges and troughs are present along the shelf centerline, with transverse (across-flow) ridges and troughs along the lateral margins (Figure 1). Local basal melt rates vary considerably across these features (Dutrieux et al., 2013; Shean, 2016).

Hydrographic observations seaward of the PIG calving front in Pine Island Bay suggest that basal melting declined by ~50% between 2010 and 2012 (Dutrieux et al., 2014). Long-term 2009–2015 mooring records seaward of the southern calving front (Figure 1) show a significant decrease in ocean temperature (~1–1.5°C) over ~450–770 m depths from late 2011 to early 2012, and then again from mid-2012 to early 2013 (Christianson et al., 2016; Webber et al., 2017). These observations show that the ocean heat content at the PIG ice-shelf front varies considerably over monthly to interannual timescales.

1.2 PIG GPS sites

Several long-term GPS stations were installed on the PIG shelf as part of a larger investigation of ice-sheet, ice-shelf, and ocean dynamics (Bindschadler et al., 2011; Stanton et al., 2013). During the early part of this effort, two GPS

stations continuously collected data from January 2008 to January 2010: one on the southern PIG ice shelf (PIG2) and another on the fast-flowing, grounded ice upstream of the grounding line (PIG1) (Figure 1). In addition, a ~2x2 km array of five stations (SOW1–4, BOAR, Figure 2) was installed ~50 km downstream of the grounding line, near the center of the main shelf from January 2012 to late December 2013.

The stations used dual-frequency Trimble NetRS GPS receivers (2008–2010 sites) and NetR9 receivers (2012–2014 sites), with Trimble Zephyr Geodetic 2 antennas mounted on 12-foot (3.66 m) poles with insulating pole-base stoppers. The poles were driven into the snow by hand, with initial pole bases set ~0.5–1.0 m beneath the surface (M. Truffer, personal communication, 2016).

High-resolution optical imagery and DEM data (see Section 2.5) over the 2012–2014 sites show that SOW1, BOAR, and SOW3 were installed with along-flow orientation in a longitudinal surface trough (Figure 2) that overlies a longitudinal basal channel. An ice-penetrating radar profile with transverse orientation was collected upstream of the GPS array, providing ice thickness estimates of ~450–460 m near the apex of a longitudinal channel and ~540 m over adjacent keels (Stanton et al., 2013). Figure 2 shows estimated ice thickness for longitudinal and transverse profiles across the GPS array.

A borehole was drilled through the ice shelf approximately 1.34 km upstream of SOW1 (K. Riverman, personal communication, 2016), and an instrument package with an upward-facing ice-bottom altimeter (acoustic ranger) was deployed beneath the shelf from January to February 2012. Measurements from this bottom altimeter and complementary pRES experiments provided basal melt rate estimates of ~14–25 m/yr within the longitudinal channel (Christianson et al., 2016; Stanton et al., 2013).

The 2012–2014 GPS array was located near several transverse surface depressions (Figure 2), which are likely associated with transverse basal channels and/or rifts. Local surface slopes were ~0.6–0.9° within the largest of these depressions, immediately downstream of SOW3 and SOW4. A notable linear surface depression located approximately 1 km upstream of SOW1 (black arrow in Figure 2) opened as a rift in ~2014 (R1 in Jeong et al. (2016)), and was subsequently the site of a large iceberg calving event that occurred around July 2015. The placement of the 2012–2014 GPS array near these features complicates interpretation of GPS records, but also provides new constraints on the spatiotemporal evolution of strain rates and rift formation for the PIG shelf.

Deleted: fortuitous

Deleted: (co)

2 Data and Methods

2.1 GPS antenna position

As described in Christianson et al. (2016), GPS data were processed using differential-carrier-phase positioning relative to bedrock GPS sites (Backer Island [BACK, -74.26°N, -102.28°E, ~60 km baseline] for 2012–2014 records; Howard Nunatak [HOWN, -77.31°N, -8.65°E, ~450 km baseline] for 2008–2010 records) with epoch-by-epoch zenith tropospheric delay estimation. Daily-averaged positions of these base stations were calculated using GAMIT and stabilized relative to a fixed circum-Antarctic reference frame using a Kalman filter (GLOBK, (Herring et al., 2015)). Antenna positions relative to the WGS84 ellipsoid were calculated every 30 seconds. We analyzed a subset of these positions sampled at 10-minute intervals, and removed any positions with uncertainty >8 cm. The BOAR record was

curtailed on April 29, 2013 (1.31 year duration), when an abrupt ~2.0 m elevation decrease and corresponding horizontal offset occurred, suggesting that the pole fell over.

We estimate initial antenna position accuracy of ~1 cm. Positions were converted to a local Cartesian horizontal coordinate system with final antenna elevation values (z_{ant}) as orthometric height above the EGM2008 geoid (Pavlis et al., 2012). Absolute geoid errors are poorly constrained for coastal Antarctica, but relative geoid error for the cumulative horizontal displacement of the GPS array (~8 km over the 2-year period) should be <1-2 cm. A constant offset of 3.71 m (3.66 m pole length + 0.053 m phase center to bottom of antenna) was removed from antenna elevation (z_{ant}) to estimate corresponding pole-base elevation.

We estimated vertical tidal displacement for all GPS positions on the PIG ice shelf using CATS2008A, an updated version of the model described by Padman et al. (2002). We used mean sea level pressure values from the 0.75°-grid-cell ERA-Interim reanalysis products (Dee et al., 2011) to correct for vertical displacement due to the inverse barometer effect (IBE, e.g., Padman et al., 2003). To do this, we removed the 2002–2016 median (985.21 hPa) from 6-hour sea level pressure and scaled the residuals by ~1 cm/hPa. Figure 3 shows that tidal amplitudes for the GPS sites range from approximately -0.9 to +1.3 m and IBE amplitudes range from -0.3 to +0.3 m. These signals were removed from the GPS antenna elevation (z_{ant}), and residual high-frequency noise was removed with a low-pass filter (1.5-day cutoff), yielding smoothed time series for further analysis (Figure 3). We conservatively estimate final z_{ant} absolute accuracy of ~0.1 m.

Deleted: along

Deleted: ~

Deleted: GPS paths

Deleted: the CATS2008A model (Padman et al., 2002).

Deleted: for the 10-minute GPS positions

2.2 Antenna-surface distance

The GPS interferometric reflectometry method (GPS-IR) provides a precise measurement of antenna phase-center height above the reflecting surface (Larson, 2016). The reflecting surface for PIG is the interface between the atmosphere and the snow/firn surface, and we define the antenna height above this interface as the "antenna-surface distance" ($h_{ant\text{-}surf}$). Figure 4 shows a schematic of this GPS site geometry.

Assuming that the GPS pole base remains fixed within its original firn layer (see Section 5.3 for further discussion), observed decreases in the antenna-surface distance ($h_{ant\text{-}surf}$) can be attributed to surface accumulation (e.g, snowfall, deposition of snow by wind). Conversely, an increase in antenna-surface distance can be attributed to surface ablation (e.g., melt, sublimation, removal of snow by wind) and compaction of snow/firn above the pole base.

We computed mean daily antenna-surface distance for all sites using L1 C/A code multipath surface reflections and the GPS interferometric reflectometry methodology outlined in Larson et al. (2015). This method takes advantage of the fact that the interference between the direct and reflected GPS signals produces characteristic frequencies in signal-to-noise ratio data recorded by the GPS receiver; these frequencies are directly related to the distance between the GPS antenna phase center and the reflecting surface. Geodetic antennas are designed to suppress multipath, so these interference patterns are best resolved at low GPS satellite elevation angles. Reflector height solutions were calculated for elevation angles of 5–25°, which sample the surface within a radial extent of ~5–50 m. Local surface slopes at each site are negligible, eliminating the need for an azimuthal correction (e.g., Larson and Nievinski, 2013). Daily antenna-surface distance ($h_{ant\text{-}surf}$) accuracy is estimated to be ~1 cm (Larson et al., 2015).

2.3 GPS-derived surface elevation

The antenna-surface distance ($h_{ant\text{-}surf}$) was subtracted from antenna elevation (z_{ant}) to obtain daily records of surface elevation z_{surf} (i.e., elevation of air-snow/firn interface above EGM2008 geoid), with resulting relative accuracy of ~1-2 cm (absolute accuracy subject to the same ~0.1 m z_{ant} uncertainty due to tidal, IBE, and geoid corrections). The z_{surf} surface elevation values are directly comparable with satellite/airborne laser altimetry data and stereo DEM products. We use variable name z_{surf} rather than the more traditional glaciological variable name h to limit potential confusion between different "height" and "elevation" variables.

Continuous z_{surf} time series were generated for all seven PIG GPS sites. The SOW3 record was curtailed on August 22, 2013, when antenna-surface distance decreased below the minimum threshold of ~0.5 m (Nievinski, 2013).

2.4 GPS velocity and strain rate

Horizontal velocities for each GPS station were computed from daily mean antenna positions. We calculated principal strain rates for 8 different triangular sections within the array (each defined by unique combination of 3 sites), using the methods outlined by Savage et al. (2001). We tested multiple time intervals for these strain rate calculations, from 2 to 120 days, and use 42 days as a compromise between temporal resolution and uncertainty (assuming uncorrelated daily position error of ~1 cm). We used observed horizontal strain rates to estimate elevation change related to local flux divergence.

Some component of observed GPS surface elevation change may also be related to deformation due to local gradients in the driving stress and surface-parallel flow due to advection over basal topography. The vertical component of surface-parallel flow (V_0 in Larson et al. (2015)) can be estimated using observed horizontal GPS paths and surface gradients from an independent DEM. Advection over bed topography is irrelevant for a freely-floating ice shelf, and we attempt to estimate an upper bound for V_0 due to local deformation by considering local surface gradients and observed relative horizontal displacements within the 2012–2014 GPS array.

2.5 High-resolution DEMs

In addition to the GPS elevation data, we generated WorldView/GeoEye stereo DEMs (Shean et al., 2016) with 32-m posting over the PIG shelf (Shean, 2016) to provide spatial context for the GPS time series. A total of 7 WorldView DEMs intersected the 2012–2014 GPS positions. We sampled DEM surface elevation at corresponding GPS positions and compared with GPS-derived surface elevation where possible.

Deleted: between 2012–2014

High-resolution Lagrangian Dz_{surf}/Dt maps (see methodology in Shean, 2016; note we use D/Dt to indicate a Lagrangian differential operator) were computed for the 2012–2014 GPS sites by forward-propagating 32-m DEM pixels from two initial DEM products (February 2, 2012 and October 23, 2012) using interpolated, time-variable surface velocity maps from Joughin et al. (2010) and Christianson et al. (2016). Lagrangian Dz_{surf}/Dt maps were generated for all valid combinations of these initial DEMs and ~15 subsequent DEMs (~0.5–2.5 years later). Composite products were generated, with median Dz_{surf}/Dt values assigned to initial DEM pixel locations.

2.6 Surface mass balance

We analyzed estimates of 1979–2015 monthly and 2010–2013 daily SMB for three 27-km grid cells over the PIG shelf from the Regional Atmospheric Climate Model (RACMO) v2.3 (Ettema et al., 2009; Lenaerts et al., 2012; Van Meijgaard et al., 2008; Van Wessem et al., 2014). The average 1979–2015 SMB ($\bar{a}$) is 0.91 m w.e./yr for the grid cell closest to the 2012–2014 GPS array (-75.07°N, -100.80°E, Figure 1). The values for adjacent grid cells are 0.74 m w.e./yr near the grounding line of the main shelf (-75.15°N, -99.88°E) and 0.84 m w.e./yr over the south shelf (-75.30°N, -101.14°E), providing some information on large-scale spatial variability. These values are consistent with SMB estimates of ~0.5–1.0 m w.e./yr derived from CReSIS Snow Radar data collected upstream of the PIG grounding line (Medley et al., 2014, 2015) and SMB estimates of 0.99 and 1.06 m w.e./yr for stake measurements near 2006–2008 GPS sites over the upstream PIG trunk (Scott et al., 2009). We conservatively estimate SMB uncertainty of 0.2 m w.e./yr.

2.7 AWS temperature data

To provide context for surface elevation change due to surface melt events, we analyzed continuous 2011–2015 temperature data (3-hour interval) from the Evans Knoll (-74.85°N, -100.40°E, Figure 1) automated weather station (AWS) (Lazzara et al., 2012), located at an elevation of ~178 m (height above EGM2008 geoid) on a bedrock outcrop approximately 40 km north of the 2012–2014 GPS array (Figure 1). We also analyzed local New York University (NYU) AWS temperature data available near PIG2 from January 9, 2008 to November 7, 2009, and near BOAR from January 19, 2013 to May 26, 2015. Unfortunately, no AWS data were collected on the PIG shelf during 2012. An analysis of overlapping time periods for the Evans Knoll and 2013-2015 NYU AWS temperature records shows a median offset of +1.24°C (Evans Knoll warmer than NYU, with normalized median absolute deviation [NMAD] of 2.76°C), which is consistent with a dry adiabatic lapse rate and local site conditions. This offset was removed from the Evans Knoll temperature data to provide a continuous temperature estimate for the GPS sites over the full 2012-2014 period.

To provide historical context, we extracted 2-m air temperature over the PIG shelf from 0.75°-resolution ERA-Interim reanalysis products (Dee et al., 2011) for the 1979–2015 period with 6-hour interval. The median offset between the ERA-Interim temperature data and the 2013-2015 NYU AWS temperature data was +0.10°C (ERA-Interim warmer than NYU) with NMAD 2.78°C. This median offset was removed from the ERA-Interim temperatures. We did not attempt to correct any seasonal bias in ERA-Interim products (e.g., Jones et al., 2016).

2.8 Firn model

We use a dynamic firn model to simulate elevation change related to SMB and firn processes, which can be used to isolate the component of observed elevation change related to ice dynamics and basal mass balance. Model SMB output from RACMO2.3 (Section 2.6) was used to force the semi-empirical 1-D IMAU-FDM dynamic firn model (Ligtenberg et al., 2011) with 3-hour timestep, and IMAU-FDM output was generated at 2-day intervals. Velocities (v_{ice}) across the firn-ice transition (defined as the layer with 917 kg/m^3 density) were assumed to be in equilibrium with average 1979–2015 SMB ($\bar{a}$ = 0.91 m w.e./yr), so that $v_{ice} = \bar{a}/\rho_i$. Vertical velocity components for surface

Deleted: from 1979–2015 for grid cells
Deleted: in
Moved (insertion) [1]
Deleted:).

accumulation, surface sublimation, surface snow drift erosion/deposition, surface melt, dry firn compaction, and a vertical buoyancy correction (over floating ice shelf grid cells) were computed for the 2008–2010 and 2012–2014 periods (see Ligtenberg et al. (2011) for model details). These components were combined to provide time series of simulated surface elevation ($\widetilde{z_{surf}}$) at each GPS station. In addition, simulated elevations were computed over time for tracers corresponding to the initial surface and pole base. We conservatively estimate IMAU-FDM surface elevation uncertainty of ~10%, which corresponds to ~0.05 m for $\widetilde{z_{surf}}$.

Deleted: (v_{fc}),

Deleted: (see Ligtenberg et al., 2011 for model details).

Deleted: and a tracer for pole-base elevation at each GPS station.

Deleted: and ~0.1 m/yr for v_{fc}.

3 Derivation of basal mass balance

We combine the above observations and model output to estimate basal mass balance for the PIG GPS sites. Mass conservation for a column with ice-equivalent thickness H_{ice} (after removing a thickness correction d that accounts for total air content in the firn column) relates Eulerian thickness change (dH_{ice}/dt) with dynamic thinning/thickening due to flux divergence ($\nabla \cdot H_{ice}\mathbf{u}$, positive for extension), surface mass balance $\dot{a}$ (meters ice equivalent), and basal mass balance $\dot{b}$ (meters ice equivalent, defined as positive for melt):

Deleted: integrate

$$\frac{\partial H_{ice}}{\partial t} = -\nabla \cdot (H_{ice}\mathbf{u}) + \dot{a} - \dot{b} \quad (1)$$

The material derivative definition relates Eulerian (fixed reference frame) and Lagrangian (reference frame moving with the ice column) thickness change:

$$\frac{DH_{ice}}{Dt} = \frac{\partial H_{ice}}{\partial t} + \mathbf{u} \cdot (\nabla \mathrm{H}_{ice}) \quad (2)$$

Rearranging Equation 2 and substituting into Equation 1, we obtain the mass conservation equation for Lagrangian thickness change:

$$\frac{DH_{ice}}{Dt} = -H_{ice}(\nabla \cdot \mathbf{u}) + \dot{a} - \dot{b} \quad (3)$$

For a floating ice shelf in hydrostatic equilibrium, we can estimate ice-equivalent thickness from air-column-corrected surface elevation ($z_{surf} - d$), where z_{surf} is measured surface elevation and d is total firn-air content:

Deleted: ice-equivalent

$$H_{ice} = (z_{surf} - d)\left(\frac{\rho_w}{\rho_w - \rho_i}\right) \quad (4)$$

Deleted: ≈ (z_{surf}

assuming a constant bulk density for ocean water (ρ_w=1026+/-1 kg/m^3) and ice (ρ_i= 917+/-5 kg/m^3). We substitute Equation 4 into Equation 3, and rearrange to estimate basal melt rate from observed surface elevation change:

$$\dot{b} = -\left(\frac{Dz_{surf}}{Dt} + (z_{surf} - d)(\nabla \cdot \mathbf{u})\right)\left(\frac{\rho_w}{\rho_w - \rho_i}\right) + \dot{a} \quad (5)$$

Here, we assume that the total firn-air content ($d \approx 12$ m for the PIG shelf [see appendix in Shean (2016)], with uncertainty of ~2 m) remains constant for the period dt, and drop the constant d from the material derivative term. This simplification is supported by the limited temporal variability (+/-0.3 m, or ~1-3%) in modeled IMAU-FDM total firn air content for the three PIG shelf grid cells during the relevant ~2-year study periods. We note that estimated basal melt rates are ~9 times more sensitive to surface elevation change (Dz_{surf}/Dt) than SMB ($\dot{a}$) for a floating ice shelf.

Deleted: We

The effects of processes that drive short-term surface-elevation change (e.g., accumulation, melting) are largely absent below the upper few meters of the firn column. Thus, elevation change at the GPS pole base (equivalent to Dz_{ant}/Dt for constant pole length) displays less variability than elevation change at the surface, as it is most sensitive to 1) compaction rates within the underlying firn, 2) the long-term average SMB (see Section 2.8), 3) basal mass balance, and 4) flux divergence. For the pole base depths and time periods involved in this study, the first two terms display limited to no variability, the flux divergence term is negligible, and observed Dz_{ant}/Dt can capture basal melt rate variability that might be obscured by surface accumulation/ablation signals in observed Dz_{surf}/Dt.

4

4 Results

4.1 Horizontal velocity

Figure 5A shows horizontal surface velocities of the PIG1 and PIG2 stations. On the floating ice at PIG2, velocity increased from ~355 m/yr to ~380 m/yr between 2008 and 2010 as the GPS moved downstream. Velocities for grounded ice at PIG1 increased at a relatively steady rate from ~420 m/yr to ~460 m/yr as the station moved toward the fast-flowing PIG trunk (Figure 1).

Figure 5B shows the 2012–2014 velocities for the GPS array, which varied from ~3830–4040 m/yr (Christianson et al., 2016). Velocities at SOW1, BOAR, and SOW3 were similar, while SOW4 (closer to shelf centerline) consistently moved ~20 m/yr faster than these three sites, and SOW2 consistently moved ~15 m/yr slower. Thus, there appears to be ~30–40 m/yr dextral (right-handed) shear across the ~2.4 km distance between the SOW4 and SOW2 sites. This transverse velocity gradient is also apparent in velocity mosaics (e.g., Christianson et al., 2016).

The velocity of all five stations varied by ~2–4% from 2012-2014, as described in detail by Christianson et al. (2016). In general, the stations displayed similar relative velocity evolution, with several abrupt >0.1–0.2 m/day velocity changes during the ~2-year period (Figure 5).

4.2 Strain rate

Figure 6 shows strain rate magnitude and direction for 8 different strain triangles within the 2012–2014 GPS array. Mean principal strain rates were +0.0018 yr^{-1} (extension approximately in the along-flow direction) and -0.0001 yr^{-1} (compression approximately in the across-flow/transverse direction). The array displayed a clockwise rotation rate of ~1°/yr.

Spatial variations of strain rates within the array are small (Figure 6). Strain triangles including SOW1 experienced higher strain rates, while triangles including SOW3 experienced lower strain rates, despite its location within the large transverse depression (Figure 2). Strain rate temporal variability is also limited, but there do appear to be significant changes correlated with shelf-wide velocity changes. In general, increased (decreased) extensional strain rates were observed following an increase (decrease) in absolute GPS array velocity.

Deleted: We now consider elevation change for the GPS pole base within the firn column of this simplified ice shelf.

Deleted: the

Deleted: of

Deleted: is much more

Deleted: the velocity across the firn-ice transition (v_{ice}

Moved up [1]: $= \bar{a}/\rho_i$

Deleted: ,

Deleted: compaction within the underlying firn. The downward velocity of

Deleted:

Deleted: due

Deleted: firn compaction (v_{fc}) varies as a function of pole-base depth within

Deleted: firn column. Values for v_{fc}

Deleted: estimated

Deleted: integrating firn model compaction rates from the firn-ice transition to the pole-base tracer at each timestep. If SMB ($\dot{a}$) for the time period dt is approximately equal to the long-term average SMB ($\bar{a}$), then:

Deleted: $\frac{Dz_{ant}}{Dt} \approx \frac{Dz_{surf}}{Dt} + v_{fc}$ ... [1]

Deleted: the

Local surface slopes near SOW1, SOW2, and BOAR are negligible (<0.2°), so we assume no surface-parallel vertical motion for these stations (i.e., $V_0 = 0$). If all of the observed ~3.4 m/yr relative displacement between SOW1 and SOW3 was attributed to flow down ~0.6° local surface slopes at SOW3, then the associated V_0 magnitude would only be ~0.03 m/yr, which is negligible compared to the observed ~5.2 m/yr Dz_{surf}/Dt.

For estimated ice-equivalent thickness of ~430–500 m, the observed strain rates correspond to shelf thinning rates (DH_{ice}/Dt) of ~0.5–0.9 m/yr, with expected surface elevation change (Dz_{surf}/Dt) of only <0.07–0.13 m/yr. Based on these estimates, we assume a value of -0.1 ± 0.03 m/yr for the divergence term in Equation 5.

Deleted: Equations 5 and 7 when calculating basal melt rates.

4.3 Antenna-surface distance

Initial antenna-surface distances ($h_{ant\text{-}surf}$) were ~2.5 to 3.1 m, indicating that initial pole-base depths were ~0.6 to 1.2 m below the initial surface (Figure 7A, Figure 8). Antenna-surface distance decreased over time at all sites, with $Dh_{ant\text{-}surf}/Dt$ rates of approximately -0.8 to -1.1 m/yr (Figure 7A).

Deleted: .

At both PIG1 and PIG2, there were periods of relatively rapid antenna-surface distance decrease (e.g., from May to August 2008), followed by a steady increase (e.g., August 2008 to February 2009). These changes are consistent with periods of snow accumulation followed by several months of ongoing firn compaction with limited snowfall. The 2012–2014 records show similar periods of abrupt antenna-surface distance decrease and steady increase, with more limited duration.

All GPS array records show an abrupt antenna-surface distance increase (~0.2–0.3 m) between December 2012 and January 2013, which is consistent with surface melting and/or enhanced firn compaction rates above the pole base (i.e., upper few meters of the firn column).

Deleted: in

Deleted: .

4.4 GPS antenna and surface elevation change

Trends in observed antenna elevation change (Dz_{ant}/Dt) are negative and highly linear (R^2 0.98–1.00) for all PIG shelf sites, with rates of -1.6 to -2.1 m/yr at SOW1, SOW2, and BOAR, and higher rates of -5.2 m/yr and -3.8 m/yr at SOW3 and SOW4, respectively (Figure 7B, Table 1). Observed Dz_{ant}/Dt over grounded ice at PIG1 is -7.6 m/yr, with apparent concave-downward curvature. This is consistent with V_0 expected for surface-parallel flow (see Section 2.4) and dynamic thinning over the PIG trunk associated with velocity increases in 2006–2008 GPS observations (Scott et al., 2009) and satellite records (Joughin et al., 2010; Mouginot et al., 2014).

The 2008–2010 surface elevation change (Dz_{surf}/Dt) at PIG2 is limited (-0.13 m/yr). By contrast, surface elevations decreased significantly at all 2012–2014 GPS array sites, with rates of -0.9 to -1.3 m/yr for SOW1, SOW2 and BOAR, and rates of -4.1 m/yr and -3.0 m/yr at SOW3 and SOW4, respectively.

Deleted: negligible

Residuals about these linear fits (Figure 9A+B) are small for PIG shelf sites (root mean squared error (RMSE) of 0.095 m for Dz_{ant}/Dt, and RMSE of 0.143 m for Dz_{surf}/Dt), with some seasonal to annual variability. We also note relatively abrupt (~days-weeks) elevation changes that occurred across all stations in the 2012–2014 array (e.g., -0.3 to +0.3 m anomaly during June 2012).

4.5 Surface mass balance

We consider surface elevation relative to a firn layer tracer for the initial surface elevation (z_{surf} - z_{surf0}') to estimate cumulative elevation change due to SMB after GPS installation. Observed rates were ~0.9–1.1 m/yr for 2008–2010 sites and ~0.8–0.9 m/yr for 2012–2014 sites (with SOW3 at ~1.1 m/yr) (Figure 9C).

The average RACMO SMB over the central PIG shelf from 1979 to 2015 is ~0.9 m w.e./yr. Monthly SMB climatology shows low accumulation rates of ~0.01–0.04 m w.e./month over the PIG shelf during the austral summer (November to February), and high accumulation rates of ~0.08–0.1 m w.e./month during austral winter (March to October) (Figure 9D). Daily SMB products show periods of days to weeks with increased accumulation (e.g., March 2013) that can be correlated with abrupt decreases in antenna-surface distance.

The ~3-4 week period between December 24, 2012 and January 17, 2013 was relatively warm, with calibrated AWS temperatures of ~1–5°C for most days (Figure 9E). We note that these are 2-m air temperatures, and that once surface melting commenced, actual surface temperatures would be lower, but still above freezing. The daily RACMO SMB data also show two accumulation events during the last week of December 2012 (Figure 9D), which involved rain on snow (M. Truffer, personal communication, 2016). Surface elevations decreased by ~0.2–0.3 m across the entire GPS array during this warm/rainy period (Figure 9B), which is consistent with surface melting, refreezing, and/or enhanced firn compaction rates. No corresponding short-term changes were recorded by the antenna elevations during the ~3-4 week period (Figure 9A), suggesting that the processes responsible for the observed surface changes did not affect the firn layers near the pole base (~1.5 m depth). We note that there are many warm periods between 1979-2015 with greater magnitude and duration than the December 2012 to January 2013 period in the ERA-Interim 2-m air temperatures over the PIG shelf.

4.6 Firn model

Figure 7C shows that the IMAU-FDM simulated surface elevation ($\widetilde{z_{surf}}$) ranges from -0.1 to +0.4 m from 2008–2010 and -0.2 to +0.2 m from 2012–2014. The observed $D\widetilde{z_{surf}}/Dt$ trend is +0.17 m/yr from 2008-2010, with no significant trend from 2012-2014. The magnitude and timing of the simulated surface elevation variability is consistent with the detrended observed surface elevation change (Figure 9B). The observed Dz_{surf}/Dt trends (-1 to -4 m/yr), however, cannot be explained by simulated elevation change due to SMB and firn processes (Figure 7C).

4.7 Basal melt rates

We computed basal melt rates from surface Dz_{surf}/Dt elevation change using Equation 5. The resulting melt rate estimates range from ~2 m/yr at PIG2 to ~39 m/yr at SOW3 (Table 1).

The 2012–2014 melt rate estimates show significant spatial variability. The three upstream stations (SOW1, SOW2 and BOAR) experienced lower melt rates of ~9–13 m/yr, while the downstream stations near the transverse depression (SOW3 and SOW4) experienced higher rates of ~29–39 m/yr for the same time period.

Formatted: Font:Italic

Deleted: 1979–2015 RACMO

Deleted: scaled

Deleted: Simulated downward pole-base velocities due to firn compaction (v_{fc}) were ~0.70–0.75 m/yr (Figure 7, Table 1) from 2008–2010 and 2012–2014, despite variable initial pole-base depth. A slight decrease in the compaction rate occurred over time, but the curves appear approximately linear (Figure 7B). These firn compaction rates are consistent with observed Dz_{surf}/Dt during extended periods with little or no surface accumulation.

Deleted: and antenna Dz_{ant}/Dt

Deleted: Equations

Deleted: and 7, respectively.

Deleted: –4

Deleted: –43

Deleted: , with good agreement between the two approaches

Deleted: 43

4.8 High-resolution DEMs

Figure 8 shows sampled DEM elevation compared with GPS surface elevation at each site, with statistics provided in Table 2. In general, we observe good agreement between the two datasets, with RMSE of 0.72 m and NMAD of 0.57 m for the full sample (n=25). The DEMs display a slight bias (+0.43 m) relative to the GPS surface elevation.

We observe good agreement between GPS-derived (Table 1) and DEM-derived (Table 2) Dz_{surf}/Dt trends. The shorter DEM Dz_{surf}/Dt intervals (e.g., ~1 year for SOW1 and BOAR) display larger errors than longer DEM intervals (~2 years for SOW2 and SOW3).

Figure 10 shows the composite DEM-derived Dz_{surf}/Dt maps, which provide spatial context for the GPS-derived Dz_{surf}/Dt records. Little or no elevation change was observed over longitudinal ridges, while areas within and near transverse depressions experienced enhanced thinning. This thinning was concentrated on the upstream side of the transverse depressions. The Dz_{surf}/Dt products relative to the October 23, 2012 DEM (Figure 10D) also show the spatial pattern of thinning associated with the rift that opened upstream of SOW1 in ~2014 (Jeong et al., 2016).

5 Assumptions

The methods presented in Section 2 relied on several simplifying assumptions. We now offer further discussion of these assumptions and their potential influence on our results.

5.1 Hydrostatic equilibrium

In the absence of direct ice thickness measurements (e.g., radar profiles near PIG GPS sites), we assume hydrostatic equilibrium and use surface elevation to estimate freeboard ice thickness - a standard practice for ice shelf studies. While this assumption can lead to increased uncertainty within a few ice thicknesses of the grounding line (Brunt et al., 2010; Griggs and Bamber, 2011), it is reasonable for the mid-shelf location of the GPS array, which in ~2012, had been approaching hydrostatic equilibrium for over 10–12 years since crossing the grounding line.

Previous studies using airborne ice-penetrating radar data have noted that most of the PIG shelf is generally near hydrostatic equilibrium (Bindschadler et al., 2011; Dutrieux et al., 2013; Vaughan et al., 2012). Dense radar grids, however, reveal narrow shelf-bottom channels, crevasses, and other features with horizontal length scales of ~10s–100s of meters that are not apparent in ice shelf surface topography (Langley et al., 2014; Vaughan et al., 2012). The thinner ice above these narrow features is partially supported by lateral bridging stresses, so that the corresponding surface elevation will appear higher than the expected freeboard surface elevation, providing erroneously large ice thickness estimates using Equation 4 (Drews, 2015; Shabtaie and Bentley, 1982; Vaughan et al., 2012).

Experiments with a high-resolution ice-flow model show that wider basal channels tend to be near equilibrium, while increased bridging stresses support ice over narrow basal channels (Drews, 2015). The PIG GPS array is ~2 km across, which is >4-5x the local ice thickness (~350-500 m). The ~1-2 km length scale of nearby longitudinal channels/keels is >2-3x the local ice thickness, with typical surface elevation difference between trough floors and adjacent ridge crests of <10 m. For the observed ice thickness, magnitude, and length scale of surface variations, and the relatively long timescales involved, we argue that the hydrostatic assumption is reasonable, and any vertical elevation change

due to evolving bridging stresses should be negligible compared to the magnitude of observed Dz_{surf}/Dt and our conservative error estimates.

5.2 SMB spatial variability

We used modeled SMB from a single RACMO2.3 grid cell to drive the IMAU-FDM dynamic firn model, and applied the result to all GPS stations. We expect SMB to vary spatially (e.g., Medley et al., 2015) due to local environmental conditions (e.g. PIG2 elevation is >400 m higher than SOW1-4 stations on the shelf) and local surface topography (e.g., km-scale ridges/troughs), which will affect near-surface winds and snow redistribution.

The larger $z_{surf} - z_{surf0}'$ values (a proxy for surface accumulation) at SOW3 (Figure 9C) indicate that greater local accumulation occurred at this site within the transverse depression (Figure 2), potentially due to preferential deposition of wind-blown snow. However, we also note that the accumulation histories of SOW4, which sits near a surface ridge crest, and the three sites located on the floor of a broad, flat surface trough (SOW1, SOW2, BOAR) appear similar (Figure 9C).

The IMAU-FDM values do not account for horizontal advection of the firn column through spatially-variable RACMO fields (accumulation, surface temperature, etc.) over time. The GPS sites over the PIG shelf are moving ~4 km/yr (Figures 1 and 5), which is nearly double the observed PIG shelf velocities from the mid-1970s (Mouginot et al., 2014). Thus, the local firn columns beneath the GPS sites likely experienced variable SMB input over their ~50-100 km horizontal path during the corresponding 1979-2015 time period. This suggests that the true firn column thickness and compaction rates may differ from the IMAU-FDM estimates. For this reason, we use a constant firn air content estimate ($d \approx 12$ +/- 2 m) derived from available airborne ice-penetrating radar two-way travel time and altimetry surface elevation measurements (see appendix A of Shean, 2016).

5.3 Pole settling/tilting

We now consider whether some of the observed Dz_{surf}/Dt could be related to settling, heating, or tilting of the GPS poles over time. We assume that the poles froze in place shortly after installation, and the contact area (~1200 cm^2 for a ~1-meter-long cylinder with ~3.8 cm diameter) with surrounding firn should be sufficient to counter the downward gravitational force. Thus, we expect that antenna elevation change (Dz_{ant}/Dt) represents rates at the base of the pole, rather than rates within an overlying firn layer.

A related consideration involves heating of the exposed pole during summer, which might lead to decoupling from the surrounding snow/firn and allow for additional penetration of the pole base within the firn. The pole base stoppers should have prevented this penetration. In addition, we do not see any indication of such settling from December 2012 to January 2013, when surface elevations decreased by ~0.2–0.3 m, but pole base elevations showed little change (Figure 9A+B). The lack of pole-base elevation change also suggests that surface meltwater did not percolate more than ~1–2 m below the surface.

Finally, we assume that the poles were installed with vertical orientation and did not tilt over time. For an initially vertical pole with length of 3.71 m (including antenna phase-center offset), a 10° tilt would introduce a -0.06 m vertical antenna elevation error (-0.03 m/yr for a 2-year period), while a 20° tilt would introduce a -0.22 m vertical error (-

Deleted: –

Deleted: the possibility that

0.11 m/yr). Thus, we expect vertical error associated with any tilting to be negligible compared to the large observed Dz_{ant}/Dt (-1.12 to -7.60 m/yr). These 10° and 20° tilts could, however, introduce horizontal errors of up to 0.64 and 1.27 m, respectively, which would affect intra-network displacement estimates and strain rate estimates. While it is possible that some minor tilting could have occurred (especially during initial months), this was not noted during servicing/removal, and the reflectometry results do not indicate any systematic change in directional antenna-surface offset.

5.4 Strain rate length scales

We estimated ~0.1 m/yr surface elevation change due to local flux divergence, assuming that the observed relative horizontal displacements are evenly distributed across the strain triangles, which have ~1–2 km edges between GPS stations. This assumption is supported by the ~1-km spatial extent of thinning signals within/near transverse depressions in the Dz_{surf}/Dt maps (Figure 10). Even if this strain is concentrated over a shorter distance (e.g., ~200 m), this contribution only increases to ~0.5 m/yr, which is still small compared to observed Dz_{surf}/Dt signals of ~3–4 m/yr. The relatively large spatial variability in Dz_{surf}/Dt values (~1 to ~4 m/yr) and lack of spatial variability in strain rates supports the assumption that the observed Dz_{surf}/Dt is primarily caused by basal melt.

6 Discussion

6.1 SMB and firn compaction

The evolution of GPS-derived surface elevation relative to a tracer for the initial surface ($z_{surf} - z_{surf0}'$) is consistent with SMB estimates ($\dot{a}$), providing qualitative validation for the RACMO SMB and IMAU-FDM results. Based on these results, we suggest that it may be possible to extract detailed SMB records for other sites using only observed GPS antenna-surface distance and simple assumptions about firn densification (e.g., Herron and Langway, 1980). The problem is further simplified for grounded ice with negligible basal mass balance rates.

The limited variability in surface elevation at PIG2 (Figure 7C) suggests that the observed 2008–2010 SMB over the South PIG shelf was approximately equal to basal melt during this period, assuming negligible velocity divergence for this location. We observe large surface elevation trends for the 2012–2014 GPS sites with no significant simulated $D\widetilde{z_{surf}}/Dt$ trend, suggesting that SMB and firn compaction during this period were consistent with average 1979–2015 SMB ($\bar{a}$) values, and that the large observed Dz_{surf}/Dt must be attributed to other processes, specifically basal melting.

6.2 Residual elevation variability

The detrended surface (Figure 9A) and antenna (Figure 9B) elevation residuals appear unrelated. This suggests that seasonal surface processes (e.g., accumulation influencing near-surface compaction rates) are not responsible for driving antenna elevation variability. We considered several possible sources for the observed sub-annual elevation variability, including ocean (e.g., currents, sea surface height), atmospheric (e.g, pressure, temperature), and dynamic

Deleted:) combined with estimates of downward velocity due to firn compaction (v_{fc}),

Deleted: If we assume a near-surface bulk snow/firn density of ~500 kg/m^3, the ~0.7–0.9 m w.e./yr RACMO SMB estimates correspond to a surface elevation increase of ~1.4–1.8 m/yr. Combining these rates with a ~0.7–0.75 m/yr surface elevation decrease due to firn compaction provides estimates similar to observed $z_{surf} - z_{surf0}'$ trends of ~0.8-1.1 m/yr.

Deleted: The fact that we observe similar trends for Dz_{surf}/Dt and ($Dz_{ant}/Dt - v_{fc}$) (Table 1) also supports the assumption that 2008–2010 and 2012–2014 SMB ($\dot{a}$) is consistent with long-term 1979–2015 SMB ($\bar{a}$) and associated firn-compaction rates.

Deleted: in balance with ongoing firn compaction and

Deleted: .

Deleted: observed

Deleted: long-term

Deleted: to be uncorrelated.

processes (e.g, resistive stress from sea ice and/or mélange in shear margins). Unfortunately, we were unable to definitively determine the cause(s) for these variations in the ~2 year GPS records.

Some of the short-term (days-weeks) variability (e.g. June 2012) observed across all five 2012–2014 stations (Figure 9B) could be related to insufficient or incorrect IBE correction. The magnitude and timing of these systematic anomalies, however, suggests that they are likely related to grounding/ungrounding events (e.g., Joughin et al., 2016).

6.3 Strain rate history, rifting, and grounding evolution

The lateral shear across the GPS array is consistent with increased longitudinal extension closer to the PIG centerline, potentially due to locally enhanced ductile deformation (i.e., "necking" (Bassis and Ma, 2015)) across transverse depressions, and/or expansion of basal/surface crevasses and rifts. The SOW3 station, which lies within a large transverse depression (Figure 2), displays a slight acceleration in antenna elevation change (Figure 9A), potentially due to increased local extension within the depression.

An upstream regrounding event would slow ice upstream of the GPS array, initially resulting in increased extensional strain rates across the transverse rifts/depressions, followed by a velocity decrease at the GPS array. Conversely, an upstream ungrounding event would initially lead to decreased extensional strain rates across the transverse rifts/depressions, followed by an increase in observed GPS velocities. We suggest that an upstream regrounding event (Joughin et al., 2016) in ~June 2012 could be responsible for increased strain rates across the GPS array (Figure 6). Similarly, an ungrounding event in ~April 2013 followed by a grounding event in ~November 2013 could explain the decrease and subsequent increase in strain rates.

There is an abrupt ~0.1–0.2 m antenna elevation (z_{ant}) decrease at both SOW3 and SOW4 in late 2013, near the end of the records (Figure 9A). No surface elevation (z_{surf}) information is available at SOW3 due to missing antenna-surface distance data for this period (see Section 2.3), but a corresponding surface elevation decrease is observed at SOW4 (Figure 9B). These elevation decreases do not appear to be related to site servicing. Rather, these observations are consistent with relatively abrupt local extension within the transverse depression affecting SOW3 and SOW4, but not the upstream GPS sites. The timing of this event corresponds with observed lengthening of the large rift (R1) upstream of SOW1 (Jeong et al., 2016), supporting the hypothesis that relatively rapid, localized extension occurred across the transverse depressions and rifts during this period.

Deleted: ,

6.4 Comparison with *in-situ* basal melt rate observations

The GPS-derived basal melt rate estimates (~9-13 m/yr for SOW1, SOW2 and BOAR sites) appear consistent with those from bottom altimeter (~14.7 m/yr from January–February 2012) and pRES (~15–25 m/yr) measurements of Stanton et al. (2013). These measurements provide some validation for the GPS results, as they are not influenced by surface mass balance and firn processes. A direct comparison may be imprudent, however, as the Stanton et al. (2013) borehole was ~1.34 km upstream of SOW1 (near the R1 rift), which likely affected local melt rates, and we observe considerable ~km-scale spatial variability in melt rates across GPS array. Furthermore, the bottom altimeter sampled a ~5 cm diameter spot with unknown upstream/downstream orientation, approximately 30–40 cm from the edge of the 20 cm borehole. Aside from local melt variability expected due to turbulent flow near the altimeter pole or borehole

edge, the altimeter provided a relatively small spatial sample compared to the GPS results, which are sensitive to changes in a column of ice with much larger footprint (100s of meters).

6.5 Basal melt rate spatial variability

The GPS records at SOW1, SOW2, and BOAR show similar Dz_{surf}/Dt rates and residuals, which is consistent with their apparent orientation on the same "block" between transverse rifts/depressions (Figure 2), and supports the hypothesis that they were exposed to similar sub-shelf circulation. The DEM Dz_{surf}/Dt maps show enhanced surface elevation change rates, and thus higher basal melt rates, on the upstream side of transverse depressions (Figure 10), which is consistent with increased Dz_{surf}/Dt observed at the SOW3 and SOW4 sites.

This relationship is potentially related to enhanced buoyant flow and/or turbulence over increased basal slopes (e.g., Jenkins, 2011) beneath transverse surface depressions. We also suggest that these transverse basal channels may offer conduits for meltwater flow between adjacent longitudinal channels, potentially leading to increased circulation velocity and higher melt rates within the transverse depressions.

6.6 Basal melt rate sensitivity to ocean temperature variability

Christianson et al. (2016) suggest that the subtle (~2–4%) changes in 2012–2014 GPS velocity display a lagged correlation with observed variations in ocean temperature records from moorings in Pine Island Bay (see Figure 1 for location), potentially implying causality. Our analysis supports the alternative Christianson et al. (2016) hypothesis that these velocity variations are primarily related to upstream grounding evolution (Joughin et al., 2016), and extension across a series of transverse depressions.

Deleted: The 2012–2014 GPS data reveal subtle (~2–4%) changes in velocity over time that appear to

Deleted: (Christianson et al., 2016) (see Figure 1 for location).

Rates of antenna and surface elevation change (Dz_{ant}/Dt and Dz_{surf}/Dt) were essentially constant in time, with no significant variation in inferred basal melt rates during this 2-year time period. If sub-shelf melt rates beneath the GPS array covaried with observed ocean heat content beyond the shelf front in Pine Island Bay (Christianson et al., 2016; Webber et al., 2017), a significant change in both Dz_{ant}/Dt and Dz_{surf}/Dt would be expected during this period. The lack of any significant deviation suggests that melt rates at these sites were not noticeably affected by observed ocean temperature variability. This finding suggests that either: 1) these sites are not representative of melt rates for the inner shelf (e.g., those near the grounding line), 2) the oceanographic measurements near the PIG ice front are not representative of water circulating beneath these ice-shelf sites, and/or 3) local melt rates are less sensitive to the observed oceanographic changes than previously assumed.

Deleted: for this 2-year time period. If sub-shelf melt rates beneath the GPS array covaried with ocean heat content beyond the shelf front in Pine Island Bay, and had decreased by ~50% as suggested by Dutrieux et al. (2014), a significant change in both Dz_{ant}/Dt and Dz_{surf}/Dt would be expected during this period.

6.7 Future work

High-resolution velocity maps derived from sub-meter imagery could potentially constrain local velocity divergence and length scales for observed strain between GPS receivers. In addition, seismic data from stations deployed near the GPS array and regional sites could help constrain the timing and location of rift propagation and grounding/ungrounding events.

High-resolution (<1-km grid) SMB output and improved dynamic firn model output would likely offer an improved understanding of local variability across the GPS array. It may also be possible to further constrain firn-compaction

rates, and thus long-term SMB, using relative layer thicknesses observed in CReSIS snow radar measurements (e.g., Medley et al., 2015) or *in-situ* pRES observations (e.g, Jenkins et al., 2006). However, airborne radar data over the PIG shelf suffer from clutter due to km-scale surface/basal topography and crevasses, while the available intermittent pRES records (Stanton et al., 2013) likely lack the sensitivity to detect small changes in firn layer thickness during the ~3-week observation period.

These limitations highlight the current value of long-term GPS records to constrain surface evolution where observations are sparse and model results are poorly constrained. Expanding the scope of our study to include the full archive of geodetic GPS data for the Antarctic and Greenland ice sheets would offer a valuable new dataset for calibration/validation of models and remote sensing data.

We offer the following recommendations to improve GPS interferometric reflectometry results for future GPS deployments: 1) set the GPS elevation mask to 0° (default values are typically ~5–10°), 2) track all possible signals (L2C, L5, Galileo, and GLONASS), 3) ensure that antenna-surface distance will remain >0.5 m between servicing visits, and 4) document and photograph GPS sites, noting antenna-surface distance and any pole tilt during install and servicing.

7 Summary and conclusions

We analyzed GPS records for the PIG shelf for the 2008–2010 and 2012–2014 periods. We produced daily time series of antenna-surface distance ($h_{ant\text{-}surf}$) and antenna elevation (z_{ant}, relative to EGM2008 geoid), which were combined to accurately measure surface elevation (z_{surf}) at each site. The surface elevation data can be directly compared with remote-sensing measurements, providing independent validation for high-resolution WorldView stereo DEM records (RMSE of ~0.72 m, NMAD of ~0.57 m).

The GPS-derived surface elevation data provide new information about local SMB that can be compared with coarse-resolution model output and AWS data. Surface elevation relative to a firn layer tracer for the initial surface (z_{surf} - $z_{surf(t_0)}$) increased at rates of ~0.8–1.1 m/yr for all GPS sites, which is consistent with modeled SMB of ~0.7–0.9 m w.e./yr. An abrupt ~0.2–0.3 m surface elevation decrease, likely due to surface melt and/or enhanced firn compaction, is observed across all GPS sites during a period of warmer atmospheric temperatures from December 2012 to January 2013.

Trends in observed antenna (Dz_{ant}/Dt) and surface elevation change (Dz_{surf}/Dt) were highly linear for all GPS sites on the PIG shelf. Observed extensional strain rates were ~0.001–0.002 yr^{-1} for the 2012–2014 GPS array, which corresponds to only ~0.1 m/yr surface elevation change due to local flux divergence.

An alternative form of the mass conservation equation was used to estimate BMB from observed Lagrangian surface elevation change, strain rates, and SMB. Basal melt rates were ~10 to ~40 m/yr near the center of the fast-flowing PIG shelf, and ~2 m/yr for the southern shelf. These melt rates are similar to those derived from complementary *in-situ* instrument records (Stanton et al., 2013) and high-resolution stereo DEMs (Shean, 2016).

Both GPS and DEM records show higher basal melt rates within and near transverse surface depressions and rifts associated with longitudinal extension. Basal melt rates for the 2012–2014 period show limited temporal variability, despite substantial changes in ocean heat content at the ice front and likely in the ice-shelf cavity. Residual elevation

Deleted: cal/val

Deleted: °,

Deleted: from

Deleted: and modeled downward firn-compaction velocities (v_{fc}) of ~0.70–0.75 m/yr

Deleted: Similar rates with reduced residual variability were obtained after removing simulated pole-base firn-compaction velocity (v_{fc}) from antenna elevation change (Dz_{ant}/Dt), which provides further validation for firn model results. Extensional

Deleted: –4

Deleted: significant

change variability is likely related to upstream grounding/ungrounding events and the local evolution of transverse depressions/rifts. Our results demonstrate the value of long-term GPS records and interferometric reflectometry for constraining ice shelf mass balance estimates.

Acknowledgements

D. Shean was supported by a NASA NESSF fellowship (NNX12AN36H). K. Christianson was supported by NASA grants NNX16AM01G and NNX12AB69G and NSF grant 0732869. K. Larson was supported by NSF AGS-1449554. S.R.M. Ligtenberg was supported by an NWO ALW Veni grant (865.15.023). An NSF OPP grant to CReSIS (ANT-0424589) provided support for I. Joughin and additional support for D. Shean. D. Holland and M. Bushuk acknowledge support from NSF grant PLR- 0732869 and NYU Abu Dhabi grant G1204. H. Conway provided useful feedback on an earlier version of this manuscript and discussions with P. Dutrieux helped guide interpretation. M. van Wessem, P. Kuipers Munneke, and M. van den Broeke provided RACMO SMB products. The AWS data are available from the University of Wisconsin-Madison Automatic Weather Station Program (NSF ANT-1245663). We acknowledge the substantial effort required to obtain the GPS data used in this study, involving multiple PIG field campaigns led by R. Bindschadler and M. Truffer, with significant contributions from many others. We acknowledge GPS data collection and archiving provided by the UNAVCO Facility with support from NSF and NASA under NSF Cooperative Agreement No. EAR-0735156. Resources supporting the DEM generation were provided by the NASA High-End Computing (HEC) Program through the NASA Advanced Supercomputing (NAS) Division at Ames Research Center. We thank L. Padman and an anonymous reviewer for their comments/suggestions, which significantly improved this manuscript.

References

Andreassen, L. M., Elvehøy, H., Kjøllmoen, B. and Engeset, R. V.: Reanalysis of long-term series of glaciological and geodetic mass balance for 10 Norwegian glaciers, The Cryosphere, 10(2), 535–552, doi:10.5194/tc-10-535-2016, 2016.

Arthern, R. J., Vaughan, D. G., Rankin, A. M., Mulvaney, R. and Thomas, E. R.: In situ measurements of Antarctic snow compaction compared with predictions of models, J. Geophys. Res., 115(F3), doi:10.1029/2009JF001306, 2010.

Bassis, J. N. and Ma, Y.: Evolution of basal crevasses links ice shelf stability to ocean forcing, Earth Planet. Sci. Lett., 409, 203–211, doi:10.1016/j.epsl.2014.11.003, 2015.

Bindschadler, R., Vaughan, D. G. and Vornberger, P.: Variability of basal melt beneath the Pine Island Glacier ice shelf, West Antarctica, J. Glaciol., 57(204), 581–595, 2011.

Bindschadler, R. A.: History of lower Pine Island Glacier, West Antarctica, from Landsat imagery, J. Glaciol., 48(163), 536–544, 2002.

Brunt, K. M., Fricker, H. A., Padman, L., Scambos, T. A. and O'Neel, S.: Mapping the grounding zone of the Ross Ice Shelf, Antarctica, using ICESat laser altimetry, Ann. Glaciol., 51(55), 71–79, 2010.

Christianson, K., Bushuk, M., Dutrieux, P., Parizek, B. R., Joughin, I. R., Alley, R. B., Shean, D. E., Abrahamsen, E. P., Anandakrishnan, S., Heywood, K. J., Kim, T.-W., Lee, S. H., Nicholls, K., Stanton, T., Truffer, M., Webber, B. G. M., Jenkins, A., Jacobs, S., Bindschadler, R. and Holland, D. M.: Sensitivity of Pine Island Glacier to observed ocean forcing: PIG response to ocean forcing, Geophys. Res. Lett., 43(20), 10,817-10,825, doi:10.1002/2016GL070500, 2016.

Church, J. A., Cazenave, A., Gregory, J. M., Jevrejeva, S., Levermann, A., Merrifield, M. A., Milne, G. A., Nerem, R. S., Nunn, P. D., Payne, A. J., Pfeffer, W. T., Stammer, D. and Unnikrishnan, A. S.: Sea Level Change. [online] Available from: http://www.ipcc.ch/pdf/assessment-report/ar5/wg1/WG1AR5_Chapter13_FINAL.pdf (Accessed 7 January 2015), 2013.

Dee, D. P., Uppala, S. M., Simmons, A. J., Berrisford, P., Poli, P., Kobayashi, S., Andrae, U., Balmaseda, M. A., Balsamo, G., Bauer, P., Bechtold, P., Beljaars, A. C. M., van de Berg, L., Bidlot, J., Bormann, N., Delsol, C., Dragani, R., Fuentes, M., Geer, A. J., Haimberger, L., Healy, S. B., Hersbach, H., Hólm, E. V., Isaksen, L., Kållberg, P., Köhler, M., Matricardi, M., McNally, A. P., Monge-Sanz, B. M., Morcrette, J.-J., Park, B.-K., Peubey, C., de Rosnay, P., Tavolato, C., Thépaut, J.-N. and Vitart, F.: The ERA-Interim reanalysis: configuration and performance of the data assimilation system, Q. J. R. Meteorol. Soc., 137(656), 553–597, doi:10.1002/qj.828, 2011.

Depoorter, M. A., Bamber, J. L., Griggs, J. A., Lenaerts, J. T. M., Ligtenberg, S. R. M., van den Broeke, M. R. and Moholdt, G.: Calving fluxes and basal melt rates of Antarctic ice shelves, Nature, doi:10.1038/nature12567, 2013.

Drews, R.: Evolution of ice-shelf channels in Antarctic ice shelves, The Cryosphere, 9(3), 1169–1181, doi:10.5194/tc-9-1169-2015, 2015.

Dutrieux, P., Vaughan, D. G., Corr, H. F. J., Jenkins, A., Holland, P. R., Joughin, I. and Fleming, A. H.: Pine Island glacier ice shelf melt distributed at kilometre scales, The Cryosphere, 7(5), 1543–1555, doi:10.5194/tc-7-1543-2013, 2013.

Dutrieux, P., De Rydt, J., Jenkins, A., Holland, P. R., Ha, H. K., Lee, S. H., Steig, E. J., Ding, Q., Abrahamsen, E. P. and Schroder, M.: Strong Sensitivity of Pine Island Ice-Shelf Melting to Climatic Variability, Science, 343(6167), 174–178, doi:10.1126/science.1244341, 2014.

Ettema, J., van den Broeke, M. R., van Meijgaard, E., van de Berg, W. J., Bamber, J. L., Box, J. E. and Bales, R. C.: Higher surface mass balance of the Greenland ice sheet revealed by high-resolution climate modeling, Geophys. Res. Lett., 36(12), doi:10.1029/2009GL038110, 2009.

Frezzotti, M., Scarchilli, C., Becagli, S., Proposito, M. and Urbini, S.: A synthesis of the Antarctic surface mass balance during the last 800 yr, The Cryosphere, 7(1), 303–319, doi:10.5194/tc-7-303-2013, 2013.

Gao, J. and Liu, Y.: Applications of remote sensing, GIS and GPS in glaciology: a review, Prog. Phys. Geogr., 25(4), 520–540, 2001.

Griggs, J. A. and Bamber, J. L.: Antarctic ice-shelf thickness from satellite radar altimetry, J. Glaciol., 57(203), 485, 2011.

Hamilton, G. S. and Whillans, I. M.: First point measurements of ice-sheet thickness change in Antarctica, Ann. Glaciol., 27(1), 125–129, 1998.

Hawley, R. L. and Waddington, E. D.: Instruments and Methods In situ measurements of firn compaction profiles using borehole optical stratigraphy, J. Glaciol., 57(202), 289–294, 2011.

Herring, T. A., King, R. W. and McClusky, S. C.: Introduction to GAMIT/GLOBK, [online] Available from: http://chandler.mit.edu/~simon/gtgk/Intro_GG.pdf (Accessed 23 November 2016), 2015.

Herron, M. M. and Langway, C. C., Jr.: Firn densification: an empirical model, J. Glaciol., 25, 373–385, 1980.

Jacobs, S. S., Jenkins, A., Giulivi, C. F. and Dutrieux, P.: Stronger ocean circulation and increased melting under Pine Island Glacier ice shelf, Nat. Geosci., 4(8), 519–523, doi:10.1038/ngeo1188, 2011.

Jenkins, A.: Convection-Driven Melting near the Grounding Lines of Ice Shelves and Tidewater Glaciers, J. Phys. Oceanogr., 41(12), 2279–2294, doi:10.1175/JPO-D-11-03.1, 2011.

Jenkins, A., Corr, H. F., Nicholls, K. W., Stewart, C. L. and Doake, C. S.: Interactions between ice and ocean observed with phase-sensitive radar near an Antarctic ice-shelf grounding line, J. Glaciol., 52(178), 325–346, 2006.

Jeong, S., Howat, I. M. and Bassis, J. N.: Accelerated ice shelf rifting and retreat at Pine Island Glacier, West Antarctica: Central PIG rifting and calving, Geophys. Res. Lett., doi:10.1002/2016GL071360, 2016.

Jones, R. W., Renfrew, I. A., Orr, A., Webber, B. G. M., Holland, D. M. and Lazzara, M. A.: Evaluation of four global reanalysis products using in situ observations in the Amundsen Sea Embayment, Antarctica: Amundsen Sea Reanalyses Evaluation, J. Geophys. Res. Atmospheres, 121(11), 6240–6257, doi:10.1002/2015JD024680, 2016.

Joughin, I., Smith, B. E. and Holland, D. M.: Sensitivity of 21st century sea level to ocean-induced thinning of Pine Island Glacier, Antarctica, Geophys. Res. Lett., 37(20), n/a-n/a, doi:10.1029/2010GL044819, 2010.

Joughin, I., Shean, D. E., Smith, B. E. and Dutrieux, P.: Grounding line variability and subglacial lake drainage on Pine Island Glacier, Antarctica, Geophys. Res. Lett., 43(17), 9093–9102, doi:10.1002/2016GL070259, 2016.

Langley, K., von Deschwanden, A., Kohler, J., Sinisalo, A., Matsuoka, K., Hattermann, T., Humbert, A., Nøst, O. A. and Isaksson, E.: Complex network of channels beneath an Antarctic ice shelf, Geophys. Res. Lett., n/a-n/a, doi:10.1002/2013GL058947, 2014.

Larson, K. M.: GPS interferometric reflectometry: applications to surface soil moisture, snow depth, and vegetation water content in the western United States: GPS interferometric reflectometry, Wiley Interdiscip. Rev. Water, 3(6), 775–787, doi:10.1002/wat2.1167, 2016.

Larson, K. M. and Nievinski, F. G.: GPS snow sensing: results from the EarthScope Plate Boundary Observatory, GPS Solut., 17(1), 41–52, doi:10.1007/s10291-012-0259-7, 2013.

Larson, K. M., Wahr, J. and Kuipers Munneke, P.: Constraints on snow accumulation and firn density in Greenland using GPS receivers, J. Glaciol., 61(225), 101–114, doi:10.3189/2015JoG14J130, 2015.

Lazzara, M. A., Weidner, G. A., Keller, L. M., Thom, J. E. and Cassano, J. J.: Antarctic Automatic Weather Station Program: 30 Years of Polar Observation, Bull. Am. Meteorol. Soc., 93(10), 1519–1537, doi:10.1175/BAMS-D-11-00015.1, 2012.

Lenaerts, J. T. M., van den Broeke, M. R., van de Berg, W. J., van Meijgaard, E. and Kuipers Munneke, P.: A new, high-resolution surface mass balance map of Antarctica (1979-2010) based on regional atmospheric climate modeling, Geophys. Res. Lett., 39(4), n/a-n/a, doi:10.1029/2011GL050713, 2012.

Ligtenberg, S. R. M., Helsen, M. M. and van den Broeke, M. R.: An improved semi-empirical model for the densification of Antarctic firn, The Cryosphere, 5(4), 809–819, doi:10.5194/tc-5-809-2011, 2011.

Medley, B., Joughin, I., Smith, B. E., Das, S. B., Steig, E. J., Conway, H., Gogineni, S., Lewis, C., Criscitiello, A. S., McConnell, J. R., van den Broeke, M. R., Lenaerts, J. T. M., Bromwich, D. H., Nicolas, J. P. and Leuschen, C.: Constraining the recent mass balance of Pine Island and Thwaites glaciers, West Antarctica, with airborne observations of snow accumulation, The Cryosphere, 8(4), 1375–1392, doi:10.5194/tc-8-1375-2014, 2014.

Medley, B., Ligtenberg, S. R. M., Joughin, I., Van Den Broeke, M. R., Gogineni, S. and Nowicki, S.: Antarctic firn compaction rates from repeat-track airborne radar data: I. Methods, Ann. Glaciol., 56(70), 155–166, doi:10.3189/2015AoG70A203, 2015.

Moholdt, G., Padman, L. and Fricker, H. A.: Basal mass budget of Ross and Filchner-Ronne ice shelves, Antarctica, derived from Lagrangian analysis of ICESat altimetry: Ice shelf basal melting from altimetry, J. Geophys. Res. Earth Surf., n/a-n/a, doi:10.1002/2014JF003171, 2014.

Mouginot, J., Rignot, E. and Scheuchl, B.: Sustained increase in ice discharge from the Amundsen Sea Embayment, West Antarctica, from 1973 to 2013, Geophys. Res. Lett., 41(5), 1576–1584, doi:10.1002/2013GL059069, 2014.

Nievinski, F. G.: Forward and inverse modeling of GPS multipath for snow monitoring, University of Colorado. [online] Available from: http://xenon.colorado.edu/portal/publications/Nievinski_2013_PhD.pdf (Accessed 9 December 2016), 2013.

Padman, L., Fricker, H. A., Coleman, R., Howard, S. and Erofeeva, L.: A new tide model for the Antarctic ice shelves and seas, Ann. Glaciol., 34(1), 247–254, 2002.

Padman, L., King, M., Goring, D., Corr, H. and Coleman, R.: Ice-shelf elevation changes due to atmospheric pressure variations, J. Glaciol., 49(167), 521–526, doi:10.3189/172756503781830386, 2003.

Pavlis, N. K., Holmes, S. A., Kenyon, S. C. and Factor, J. K.: The development and evaluation of the Earth Gravitational Model 2008 (EGM2008), J. Geophys. Res., 117(B4), doi:10.1029/2011JB008916, 2012.

Pritchard, H. D., Arthern, R. J., Vaughan, D. G. and Edwards, L. A.: Extensive dynamic thinning on the margins of the Greenland and Antarctic ice sheets, Nature, 461(7266), 971–975, doi:10.1038/nature08471, 2009.

Pritchard, H. D., Ligtenberg, S. R. M., Fricker, H. A., Vaughan, D. G., van den Broeke, M. R. and Padman, L.: Antarctic ice-sheet loss driven by basal melting of ice shelves, Nature, 484(7395), 502–505, doi:10.1038/nature10968, 2012.

Rietbroek, R., Brunnabend, S.-E., Kusche, J., Schröter, J. and Dahle, C.: Revisiting the contemporary sea-level budget on global and regional scales, Proc. Natl. Acad. Sci., 201519132, 2016.

Rignot, E.: Changes in West Antarctic ice stream dynamics observed with ALOS PALSAR data, Geophys Res Lett, 35(12), L12505, doi:10.1029/2008GL033365, 2008.

Rignot, E., Jacobs, S., Mouginot, J. and Scheuchl, B.: Ice-Shelf Melting Around Antarctica, Science, 341(6143), 266–270, doi:10.1126/science.1235798, 2013.

Rignot, E., Mouginot, J., Morlighem, M., Seroussi, H. and Scheuchl, B.: Widespread, rapid grounding line retreat of Pine Island, Thwaites, Smith, and Kohler glaciers, West Antarctica, from 1992 to 2011, Geophys. Res. Lett., 41(10), 3502–3509, doi:10.1002/2014GL060140, 2014.

Savage, J. C., Gan, W. and Svarc, J. L.: Strain accumulation and rotation in the Eastern California Shear Zone, J. Geophys. Res. Solid Earth, 106(B10), 21995–22007, doi:10.1029/2000JB000127, 2001.

Scott, J., Gudmundsson, H., Smith, A., Bingham, R., Pritchard, H. and Vaughan, D.: Increased rate of acceleration on Pine Island Glacier strongly coupled to changes in gravitational driving stress, The Cryosphere, 3, 125–131, 2009.

Shabtaie, S. and Bentley, C. R.: Tabular icebergs: implications from geophysical studies of ice shelves, J. Glaciol., 28(100), 1982.

Shean, D.: Quantifying ice-shelf basal melt and ice-stream dynamics using high-resolution DEM and GPS time series, Ph.D. Thesis, University of Washington, Seattle, WA, 14 July. [online] Available from: https://digital.lib.washington.edu:443/researchworks/handle/1773/36365 (Accessed 22 November 2016), 2016.

Shean, D. E., Alexandrov, O., Moratto, Z. M., Smith, B. E., Joughin, I. R., Porter, C. and Morin, P.: An automated, open-source pipeline for mass production of digital elevation models (DEMs) from very-high-resolution commercial stereo satellite imagery, ISPRS J. Photogramm. Remote Sens., 116, 101–117, doi:10.1016/j.isprsjprs.2016.03.012, 2016.

Shepherd, A., Ivins, E. R., A, G., Barletta, V. R., Bentley, M. J., Bettadpur, S., Briggs, K. H., Bromwich, D. H., Forsberg, R., Galin, N., Horwath, M., Jacobs, S., Joughin, I., King, M. A., Lenaerts, J. T. M., Li, J., Ligtenberg, S. R. M., Luckman, A., Luthcke, S. B., McMillan, M., Meister, R., Milne, G., Mouginot, J., Muir, A., Nicolas, J. P., Paden, J., Payne, A. J., Pritchard, H., Rignot, E., Rott, H., Sorensen, L. S., Scambos, T. A., Scheuchl, B., Schrama, E. J. O., Smith, B., Sundal, A. V., van Angelen, J. H., van de Berg, W. J., van den Broeke, M. R., Vaughan, D. G., Velicogna, I., Wahr, J., Whitehouse, P. L., Wingham, D. J., Yi, D., Young, D. and Zwally, H. J.: A Reconciled Estimate of Ice-Sheet Mass Balance, Science, 338(6111), 1183–1189, doi:10.1126/science.1228102, 2012.

Stanton, T. P., Shaw, W. J., Truffer, M., Corr, H. F. J., Peters, L. E., Riverman, K. L., Bindschadler, R., Holland, D. M. and Anandakrishnan, S.: Channelized Ice Melting in the Ocean Boundary Layer Beneath Pine Island Glacier, Antarctica, Science, 341(6151), 1236–1239, doi:10.1126/science.1239373, 2013.

Van Meijgaard, E., Van Ulft, L. H., Van de Berg, W. J., Bosveld, F. C., Van den Hurk, B., Lenderink, G. and Siebesma, A. P.: The KNMI regional atmospheric climate model RACMO version 2.1, Koninklijk Nederlands Meteorologisch Instituut. [online] Available from: http://www.weeralarm.nl/publications/fulltexts/tr302_racmo2v1.pdf (Accessed 31 May 2013), 2008.

Van Wessem, J. M., Reijmer, C. H., Morlighem, M., Mouginot, J., Rignot, E., Medley, B., Joughin, I., Wouters, B., Depoorter, M. A., Bamber, J. L., Lenaerts, J. T. M., De Van Berg, W. J., Van Den Broeke, M. R. and Van Meijgaard, E.: Improved representation of East Antarctic surface mass balance in a regional atmospheric climate model, J. Glaciol., 60(222), 761–770, doi:10.3189/2014JoG14J051, 2014.

Vaughan, D. G., Corr, H. F. J., Bindschadler, R. A., Dutrieux, P., Gudmundsson, G. H., Jenkins, A., Newman, T., Vornberger, P. and Wingham, D. J.: Subglacial melt channels and fracture in the floating part of Pine Island Glacier, Antarctica, J. Geophys. Res., 117(F3), doi:10.1029/2012JF002360, 2012.

Webber, B. G. M., Heywood, K. J., Stevens, D. P., Dutrieux, P., Abrahamsen, E. P., Jenkins, A., Jacobs, S. S., Ha, H. K., Lee, S. H. and Kim, T. W.: Mechanisms driving variability in the ocean forcing of Pine Island Glacier, Nat. Commun., 8, 14507, doi:10.1038/ncomms14507, 2017.

Wouters, B., Martin-Espanol, A., Helm, V., Flament, T., van Wessem, J. M., Ligtenberg, S. R. M., van den Broeke, M. R. and Bamber, J. L.: Dynamic thinning of glaciers on the Southern Antarctic Peninsula, Science, 348(6237), 899–903, doi:10.1126/science.aaa5727, 2015.

Tables

Site	Time period	Days	$D(z_{surf} - z_{surf0}')/Dt$ (m/yr)	Dz_{ant}/Dt (m/yr)	Dz_{surf}/Dt (m/yr)	$\dot{b}$ (m/yr)
PIG1	2008-1-13, 2009-9-4	601	0.93	-7.60*	-6.76*	--
PIG2	2008-1-10, 2010-1-27	747	1.12	-1.12	-0.13	2.0+/-0.9
SOW1	2012-2-10, 2013-12-23	714	0.77	-1.81	-1.13	11.5+/-1.1
SOW2	2012-2-10, 2013-12-23	714	0.85	-2.08	-1.33	13.3+/-1.2
BOAR	2012-2-10, 2013-4-29	476	0.78	-1.58	-0.91	9.4+/-1.1
SOW4	2012-2-10, 2013-12-24	714	0.86	-3.76	-3.00	29.1+/-1.7
SOW3	2012-2-9, 2013-12-24	716	1.10	-5.23	-4.10	39.4+/-2.1

Table 1: GPS station data. Fields include surface elevation change relative to tracer for initial surface $D(z_{surf}-z_{surf0}')/Dt$, antenna elevation change Dz_{ant}/Dt (equal to pole-base elevation change), surface elevation change Dz_{surf}/Dt, and corresponding ice-equivalent basal melt rate $\dot{b}$. *Note: PIG1 values over grounded ice do not include correction to remove expected Dz_{surf}/Dt due to advection along local surface slopes (V_0).

Site	DEM n	DEM dt (days)	DEM Dz_{surf}/Dt (m/yr)	GPS-DEM RMSE (m)	GPS-DEM mean (m)	GPS-DEM std (m)
SOW1	5	302*	-2.30	0.69	-0.26	0.64
SOW2	5	619	-2.03	0.76	-0.46	0.60
BOAR	4	302*	-1.69	0.86	-0.55	0.66
SOW4	5	368*	-3.35	0.75	-0.61	0.44
SOW3	6	619	-4.32	0.54	-0.30	0.45

Table 2: Statistics for WorldView DEM accuracy from comparisons with measured GPS surface elevation data. Asterisks identify records with shorter time interval and increased uncertainty.

Deleted: Dz_{ant}/Dt (m/yr)
Formatted Table
Formatted: Font:Not Italic
Deleted: ... [3]
Deleted Cells
Deleted: v_{fc} (m/yr)
Deleted Cells
Deleted: $\dot{b}$ (m/yr) ... [2]
Deleted Cells
Deleted: Dz_{surf}/Dt (m/yr)
Deleted: - v_{fc}
Deleted:) /
Deleted: -0.75
Deleted Cells
Deleted: -6.85*
Deleted: --
Deleted Cells
Deleted: --
Deleted Cells
Deleted: -0.74
Deleted: -0.38
Deleted Cells
Deleted: 4.4+/-1.4
Deleted Cells
Deleted: -0.75
Deleted: -1.06
Deleted: 10.8+/-1.5
Deleted: -0.74
Deleted: -1.34
Deleted: 13.4+/-1.5
Deleted: -0.77
Deleted: -0.81
Deleted: 8.5+/-1.4
Deleted: -0.73
Deleted: -3.03
Deleted: 29.3+/-1.9
Deleted: -0.72
Deleted: -4.50
Deleted: 43.1+/-2.4
Deleted: modeled downward pole-base vertical velocity due to firn compaction v_{fc},
Deleted: antenna Dz_{ant}/Dt after removing v_{fc}, and
Deleted: rates
Deleted: computed using equations 5 and 7, respectively.
Formatted: Font:Italic
Formatted: Font:Italic

Figures

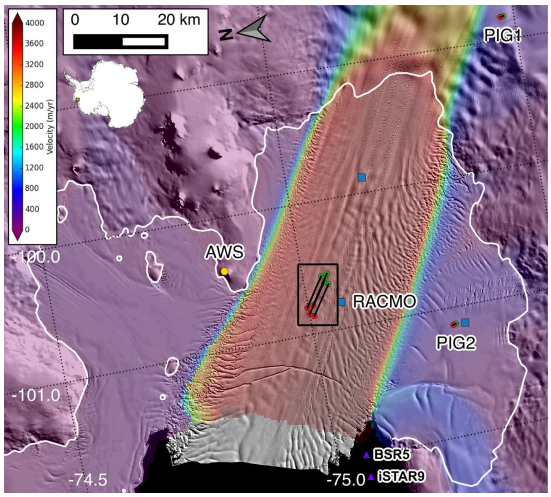

Figure 1: Context for Pine Island Glacier ice shelf with 2006–2016 median surface velocity (Christianson et al., 2016; Joughin et al., 2010) over shaded relief map from October–December 2012 DEM mosaic. Black lines show ~2-year paths between initial (green) and final (red) GPS station locations. Yellow dot shows Evans Knoll AWS and blue squares show RACMO grid cell centers used during analysis. Purple triangles beyond shelf front show locations of ocean mooring temperature data from Christianson et al. (2016). White line shows approximate 2011 grounding line (Shean, 2016). Black rectangle shows location of Figure 2A.

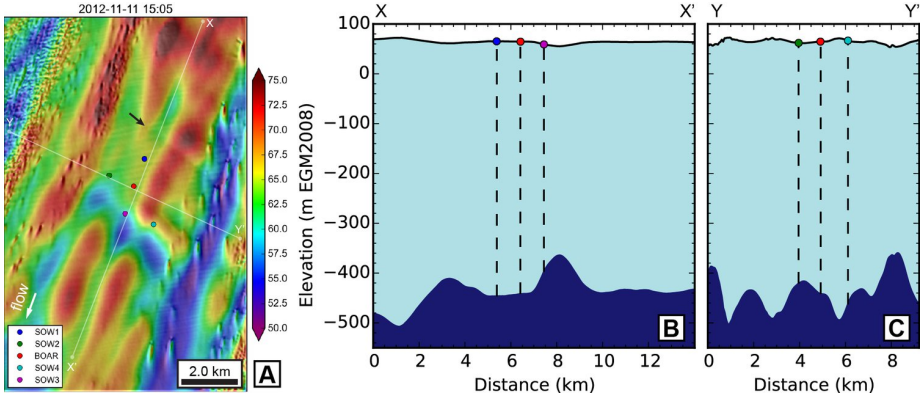

Figure 2: A) WorldView DEM from November 11, 2012 with 2012–2014 GPS array positions overlaid. Note GPS positions relative to transverse depressions and location of R1 rift associated with 2015 calving event (black arrow). Ice flow direction indicated by white arrow. White lines show locations of profiles. B) Smoothed surface elevation (0.5-km window, approx. ~1·H_{ice}) and estimated freeboard thickness for longitudinal profile X-X' and C) transverse profile Y-Y'. Profile intersection is near BOAR (red point). Vertical exaggeration is 22x.

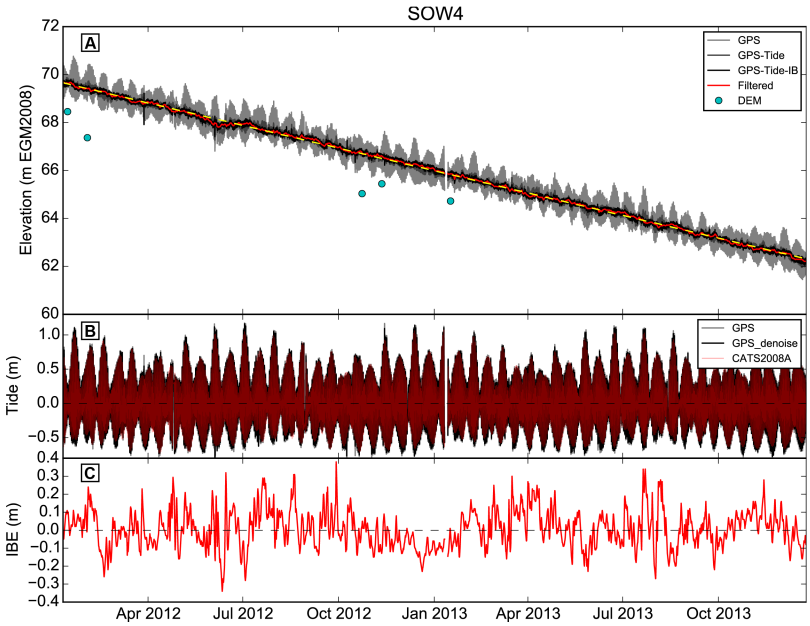

Figure 3: A) Original GPS antenna elevation (light gray), after tide correction (mid-gray), and after tide+IBE correction (black) for SOW4. Red line shows smoothed time series and yellow dashed line is linear fit (-3.76 m/yr). Sampled DEM elevations (cyan) show surface elevation, which is offset from GPS antenna elevation by antenna-surface distance (see Figures 4 and 8). B) High-frequency (<1.5 days) component of GPS record and CATS2008A tide model prediction, showing excellent agreement. C) Estimated Inverse Barometer Effect (IBE) magnitude from scaled sea-level pressure.

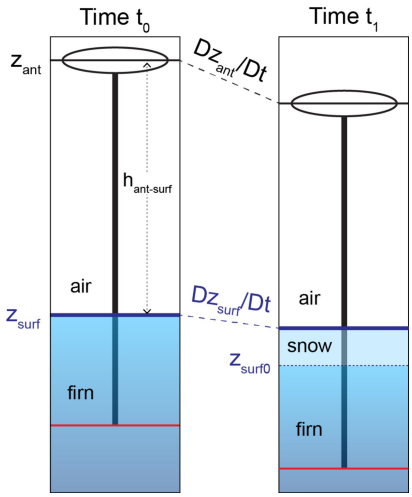

Figure 4: Schematic of GPS station geometry. Surface elevation (z_{surf}, dark blue line) is computed by removing antenna-surface distance ($h_{ant\text{-}surf}$, dotted black line) from antenna elevation (z_{ant}, black line). Pole-base elevation (red line) is computed from pole length and antenna phase-center offset. At time t_1 (right panel), ongoing firn compaction resulted in decreased antenna and pole-base elevation, while new snow accumulation offset surface lowering. The layer within the firn column corresponding to the initial surface (z_{surf0}) is represented by dotted blue line.

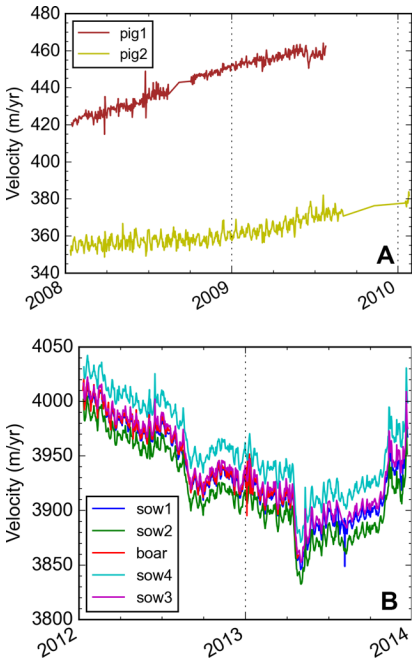

Figure 5: Station velocities derived from daily mean positions for A) 2008–2010 GPS sites, and B) 2012–2014 GPS sites. Note offset between SOW2 and SOW4, indicative of lateral shear across the ~2 km wide array, with greater extension near the center of the PIG shelf.

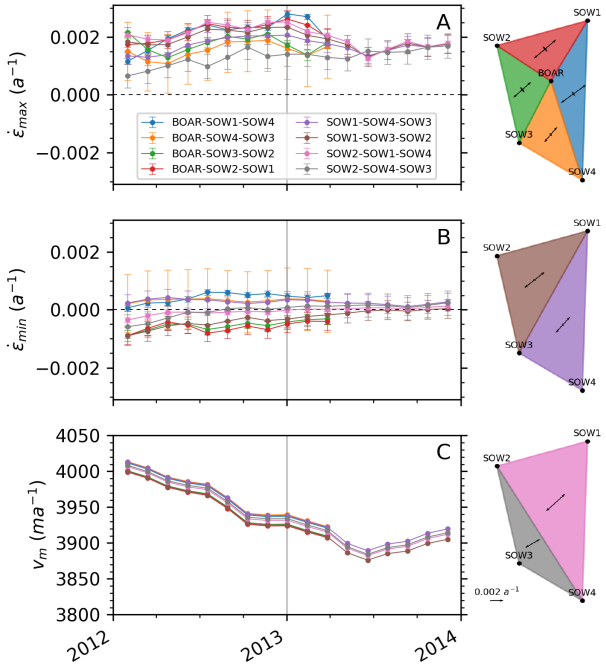

Figure 6: Horizontal strain rates over 42-day periods for 8 different triangular sections within the GPS array. A) First principal strain rate, positive for extension. Error bars calculated for uncorrelated GPS position error of 1 cm. B) Second principal strain rate. C) Velocity magnitude. Diagrams in right column show color-coded triangular sections, with ~2-year mean of principal strain rates plotted at centroids.

Deleted: Annualized velocity

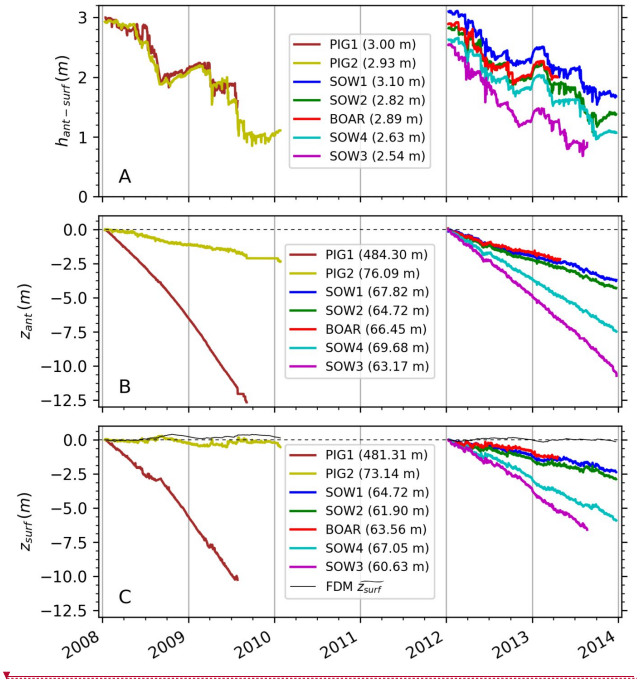

Figure 7: A) Observed antenna-surface distance ($h_{ant\text{-}surf}$) for each station. Legend lists original distance. B) Observed antenna elevation (z_{ant}) relative to initial absolute antenna elevation values listed in legend. C) Calculated surface elevation (z_{surf}) and simulated IMAU-FDM surface elevation from SMB/firn ($\widetilde{z_{surf}}$, thin black lines), both relative to initial absolute surface elevation values listed in legend.

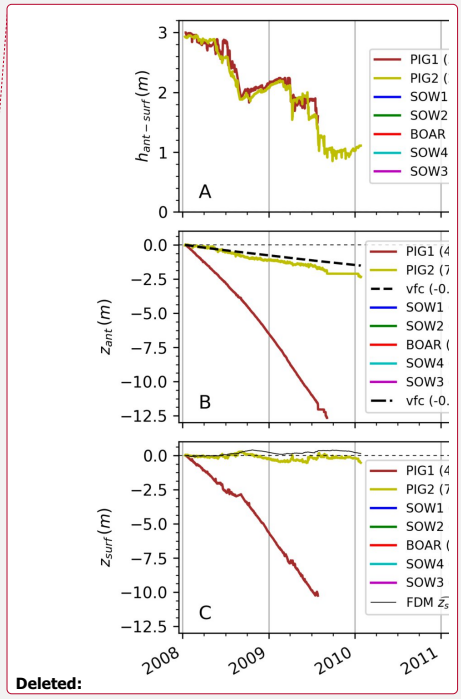

Deleted:

Deleted: Dashed black lines show modeled IMAU-FDM downward velocity due to firn compaction (v_{fc}) at the pole base.

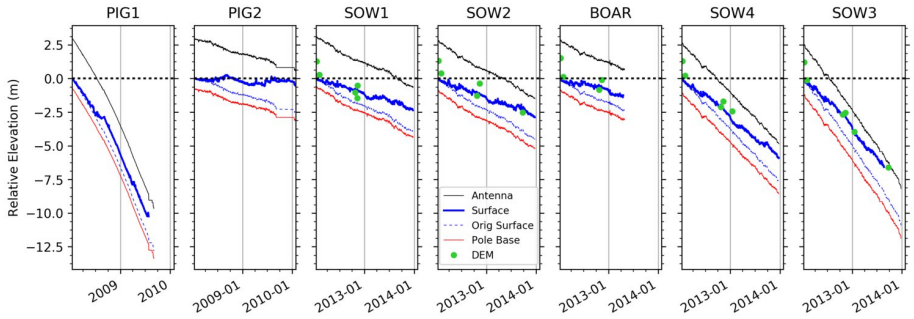

Figure 8: Time series of GPS antenna elevation (black), surface elevation (thick blue), tracer for initial surface (dotted blue), and pole-base elevation (red), all relative to initial absolute surface elevation. See schematic in Figure 4. Green points show sampled WorldView DEM surface elevation. Note surface elevation decrease at all sites but PIG2.

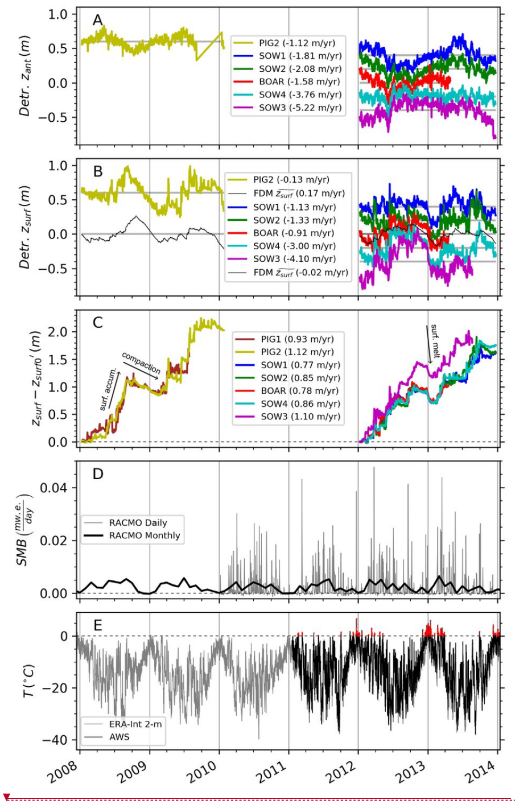

Figure 9: A) Detrended GPS antenna elevation (z_{ant}, see Figure 7B for original records), with arbitrary y-axis offset. Legend lists linear trend, which can be compared with Dz_{surf}/Dt trend in panel B (see Equation 6). B) Detrended surface elevation (z_{surf}, see Figure 7C) and detrended IMAU-FDM simulated surface elevation ($\widetilde{z_{surf}}$), with arbitrary y-axis offset. Legend lists linear trend. Note limited residual magnitude and dampened seasonal signal of z_{ant} compared to z_{surf}. Unlike z_{surf}, no significant change is observed in z_{ant} from Dec. 2012 to Jan. 2013. C) Surface elevation relative to tracer for initial surface ($z_{surf} - z_{surf0}'$). As annotated, positive slopes are indicative of new snow accumulation, shallow negative slopes indicate ongoing compaction, and steep negative slopes likely indicate surface melt. Note ~0.2–0.3 m surface decrease from December 2012 to January 2013. Legend values show linear fit at each site. D) Daily and monthly RACMO2.3 SMB. Note correlation of accumulation events and increases in panel C. E) Scaled 2-m temperature data from Evans Knoll AWS (black) and ERA-Interim (gray), with above-zero AWS temperatures plotted in red. Note extended warm period from mid-Dec. 2012 to mid-Jan. 2013, which corresponds to ~0.2–0.3 m surface elevation decrease in Panels B and C.

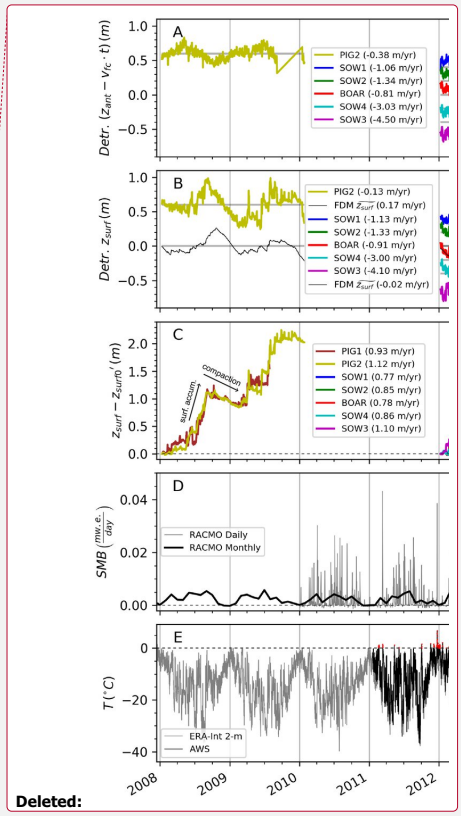

Deleted:

Deleted:) after removing v_{fc},

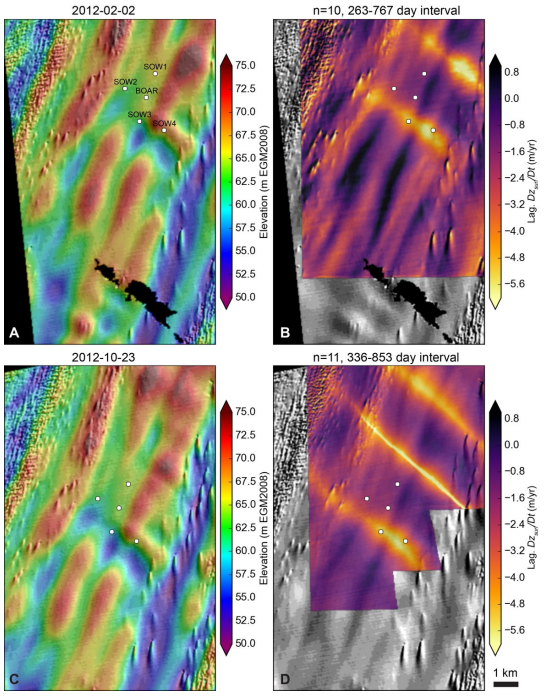

Figure 10: WorldView DEMs and composite Lagrangian Dz_{surf}/Dt products generated using A-B) initial DEM from February 2, 2012, and C-D) initial DEM from October 23, 2012. Note enhanced thinning observed within transverse depressions and rift upstream of GPS array. The Dz_{surf}/Dt maps are used to calculate basal melt rates (scaling factor of ~9, e.g., Dz_{surf}/Dt of ~1 m/yr corresponds to a basal melt rate estimate of ~9–10 m/yr)

Page 9: [1] Deleted	David Shean	9/22/17 12:31:00 PM

$$\frac{Dz_{ant}}{Dt} \approx \frac{Dz_{surf}}{Dt} + v_{fc} \quad (6)$$

which can be substituted into Equation 5 to estimate basal melt rate from observed antenna elevation change:

$$\dot{b} = -\left(\frac{Dz_{ant}}{Dt} - v_{fc} + (z_{surf} - d)(\nabla \cdot \mathbf{u})\right)\left(\frac{\rho_w}{\rho_w - \rho_i}\right) + \dot{a} \quad (7)$$

The pole-base depth below the surface is negligible compared to total ice thickness ($z_{surf} - z_{polebase} \ll H_{ice}$), and we neglect the small difference in associated firn air content.

If modeled downward velocity due to firn compaction is correct, then basal melt rate estimates from Equation 5 and Equation 7 should be similar. We also note that estimated basal melt rates are ~9 times more sensitive to surface elevation change (Dz_{surf}/Dt) than SMB ($\dot{a}$) for a floating ice shelf.

Page 24: [2] Deleted	David Shean	9/22/17 12:31:00 PM

$\dot{b}$ (m/yr)
from

Page 24: [3] Deleted	David Shean	9/22/17 12:31:00 PM

from Dz_{ant}/Dt